

# The Limitations of Brain Tumour Growth on a Chip

Timothy Duthie

Part III Project Supervisor:  
Dr Shery Huang

## Abstract

By making a macroscopic continuum approximation, a reaction-diffusion equation for the growth of cancer is derived, with the nutritional effects of glucose and oxygen being included with Michaelis-Menten reaction schemes. This model was then implemented using the finite element method, and the simulation was applied to modelling glioblastoma multiforme growth in an organ-on-a-chip system. The simulation found that the steady state distribution of cells was uniform, and the development of the cancer is qualitatively consistent with observations. Sensitivity analysis revealed that the simulation changes little with order of magnitude alterations in nutrient diffusivity, and maximal consumption rates. However, the simulation is sensitive to changes in the Michaelis constants for both glucose and oxygen, and the in diffusivity of the cancer cells. Finally, the same simulation was adapted to investigate a tumour growing *in vivo*. This confirmed that cell death will occur when a tumour reaches roughly  $2 \pm 0.5\text{mm}$ , necessitating vascularisation in living systems.

## 1 Introduction

With a survival time of less than two years, or less than one year for multifocal tumours, glioblastoma multiforme (GBM) is one of the deadliest common cancers in existence [1]. Modelling the growth of this cancer is of critical importance investigating for GCM, and eventually improving the prognosis. Many modelling approaches have been used over the years, and they can roughly be divided into two categories, continuous and discrete [2, 3]. Continuous models take a macroscopic and parametric approach, where the GBM development is described by partial differential equations (PDEs) [4] whose constants can be adjusted to fit data (but are not rigorously related to fundamental biological processes). These types of models have been well-studied and extended to include nutritional and even clinical treatment effects [5, 6, 7]. Discrete models seek a microscopic approach in which individual cells and their interactions are modelled [8]. These newer models use cellular automata methods to characterise the cancer, but fewer investigations and tests have been made.

The purpose of this investigation is to create a simulation whose parameters can be adjusted to model the growth of GBM in an organ-on-a-chip (OC) system [9]. An OC is a microfluidic device whose purpose is to mimic the conditions that would be

found in a particular tissue or organ. In our case, we are modelling a GBM OC which is created by placing cell lines of the cancer into an OC device. We have taken the continuous modelling approach where the following processes have been modelled using reaction-diffusion equations: cell motility, cancerous proliferation, cell death, glucose and oxygen limited growth. We have not modelled effects such as cell heterogeneity and evolution. Despite the fact that GMB consists of many cell genotypes which can have complex interactions [10]. We have also neglected angiogenesis, the tendency for new blood vessels to grow into late stage cancers.

An investigation of the theory is in section 2. The simulation is discussed in section 3, and its results are presented in section 4 with discussion. Final conclusions are in section 5. References and acknowledgements are in sections 6 and 7, while the code can be found in the appendix in section 8.

## 2 Background

### 2.1 Physical Model

Consider modelling the presence of cancer with a smooth scalar field of concentration  $c = c(\mathbf{r}, t)$ . We also define a cell flux vector field  $\mathbf{J} = -D_c \nabla c$ , where homogeneous and isotropic Fickian diffusion of the cells has been taken to model motility [2]. Lastly, we assert that microscopic processes result in sources and sinks in  $c$ , which can be modelled as a scalar field  $Q = Q(\mathbf{r}, c, t)$ . Suppose we take some volume  $\Omega$ , bounded by the closed surface  $\Sigma$ . The surface integral of  $-\mathbf{J}$  is the rate of cells entering  $\Omega$ , while the volume integral of  $Q$  is the rate of the number of cells produced or destroyed in  $\Omega$ . Thus we can write the change in the number of cells in  $\Omega$  across some time period as:

$$\Delta N = \int \left( - \oint_{\Sigma} \mathbf{J} \cdot d\mathbf{S} + \int_{\Omega} Q dV \right) dt.$$

Differentiating with respect to time, including Fick's law in  $\mathbf{J}$ , and noticing that a volume integral of  $c$  is the number of cells in  $\Omega$  yields:

$$\frac{\partial}{\partial t} \int_{\Omega} c dV = \oint_{\Sigma} D_c \nabla c \cdot d\mathbf{S} + \int_{\Omega} Q dV.$$

As space and time are independent, we can move the temporal differential inside the volume integral, and also apply the divergence theorem to the diffusion term:

$$\int_{\Omega} \frac{\partial c}{\partial t} dV = \int_{\Omega} \nabla \cdot (D_c \nabla c) dV + \int_{\Omega} Q dV.$$

Since  $\Omega$  is arbitrary, this must hold for any volume. We recover the reaction-diffusion model of GBM growth:

$$\frac{\partial c}{\partial t} = \nabla \cdot (D_c \nabla c) + Q. \quad (1)$$

It can be shown that this equation (for our chosen form of  $Q$ ) possesses solutions which are bounded and (for positive initial conditions) positive-definite [11].

## 2.2 Oxygen-Limited Growth

One of the simplest models of population growth is the logistic model. By taking the following form of  $Q$ , we model the self-limiting growth in the concentration.

$$Q = \alpha c \left( 1 - \frac{c}{c_m} \right),$$

where  $\alpha$  is a constant determining the rate, and  $c_m$  is the maximum concentration of cancer cells possible in the environment. In this case, the linear term models the proliferation of cancer cells, while the (negative) quadratic term models the loss in cells due to competition and non-specific nutritional effects. The combination of these terms causes the population to grow rapidly when  $c$  is small, but then slow and stop to a maximum as  $c$  tends to  $c_m$ . We must also assume that cell death does not interfere with new cell growth, that is the products of apoptosis are re-used or do not interfere with living cells.

The specific effect of oxygen has been included in the following scheme. We suppose that  $\alpha$  and  $c_m$  are functions of the rate of oxygen metabolism,  $v$ . In general we can not find the exact functional forms of  $\alpha(v)$  and  $c_m(v)$ , but to a first order approximation we can write:

$$\alpha(v) = \alpha \frac{v}{v_{o2}}, \quad (2)$$

$$c_m(v) = c_m \frac{v}{v_{o2}}. \quad (3)$$

Here  $v_m$  is the maximal rate of oxygen metabolism, such that when  $v = v_{o2}$  we recover the case where oxygen is a non-specific limiting factor for growth. Biologically speaking, we wish to capture the behaviour of nutrient-limited proliferation by reasoning that a cell undergoing a high rate of metabolism should also be able to proliferate rapidly, as it will be producing enough energy and metabolites to grow. Now we must find a model for  $v$  in order to include it into our scheme. The simplest meaningful equation for  $v$  comes from Michaelis-Menten enzyme dynamics [12]:

$$v = v_m \frac{[O_2]}{k_{o2} + [O_2]}, \quad (4)$$

where  $[O_2]$  is the concentration of oxygen, and  $k_{o2}$  is a Michaelis constant (defined as being the oxygen concentration where the rate of reaction is halved). Thus  $Q$  becomes:

$$Q = \alpha c \left( \frac{v}{v_{o2}} - \frac{c}{c_m} \right). \quad (5)$$

We notice that the linear growth term is now dependent on the metabolism, but the quadratic loss term is not.

The same derivation carried out in the previous subsection can be used to describe the diffusive evolution of  $[O_2]$ :

$$\frac{\partial [O_2]}{\partial t} = \nabla \cdot (D_{o2} \nabla [O_2]) + P. \quad (6)$$

Defining  $u = \frac{c}{c_m}$ , we choose

$$P = -v_m \frac{[O_2]}{k_{o2} + [O_2]} u, \quad (7)$$

to model the loss in oxygen due to metabolic effects in the cancer. First order dependence on  $c$  has been included in order to account for the reduction in oxygen consumption as  $c$  falls. No further source terms have been included, as oxygen sources will come from the boundary conditions of our specific problem. Combining equations (1), (5), (6) and (7) produces the system of equations:

$$\frac{\partial u}{\partial t} = D_c \nabla^2 u + \alpha u \left( \frac{[O_2]}{k_{o2} + [O_2]} - u \right),$$

$$\frac{\partial [O_2]}{\partial t} = D_{o2} \nabla^2 [O_2] - v_{o2} \frac{[O_2]}{k_{o2} + [O_2]} u.$$

Since we assume homogeneous and isotropic diffusion, the coefficients have been pulled out of the spacial differentials as they are not functions of position.

### 2.3 Glucose

Complete metabolic pathways for glucose can become very complex [6] and are beyond the scope of this project. However, one key phenomenon we model is the Warburg Effect [13]. This is the observation that cancerous cells develop most of their cellular energy from glycolysis, rather than fully aerobic respiration. Cancer cells prefer the less efficient anaerobic respiration of glucose into lactate, even when oxygen is not a limiting factor. So we can suppose that the PDEs describing the evolution of oxygen and glucose should have no explicit dependence on one another. Completing a similar derivation to the previous section (with now mixed second order dependence of  $\alpha$  and  $c_m$  on the rates) gains the system of equations:

$$\frac{\partial u}{\partial t} = D_c \nabla^2 u + \alpha u \left( \frac{[O_2]}{k_{o2} + [O_2]} \frac{[g]}{k_g + [g]} - u \right), \quad (8)$$

$$\frac{\partial [O_2]}{\partial t} = D_{o2} \nabla^2 [O_2] - v_{o2} \frac{[O_2]}{k_{o2} + [O_2]} u, \quad (9)$$

$$\frac{\partial [g]}{\partial t} = D_g \nabla^2 [g] - v_g \frac{[g]}{k_g + [g]} u. \quad (10)$$

Here  $[g]$ ,  $D_g$ ,  $v_g$ , and  $k_g$  are the concentration, diffusivity, maximum reaction rate, and Michaelis constant of glucose. More complex schemes accounting for the metabolism of lactate have been studied in the past [6, 5], and our system of equations resembles these models when lactate concentration is zero. Thus we implicitly assume that lactate does not build in sufficient quantities for its metabolism to be significant.

It is these systems of equations, 8-9-10, along with their boundary conditions (BCs) and initial conditions (ICs), which define the mathematical model used in the following sections. Since both sets of equations are highly non-linear, no separable solutions exist for either set. Although unproven, it is also unlikely that any analytical solution exists, so we must use numerical integration in order to estimate solutions.

### 3 Implementation

#### 3.1 System

Our primary concern is modelling an OC system used and studied by the Biointerface Group at the Engineering Department. It is a microfluidic device composed of a central chamber supplied by a set of inlet tubes, which are all encased in PDMS. Diagrams of this system can be found in figures 1 and 2.

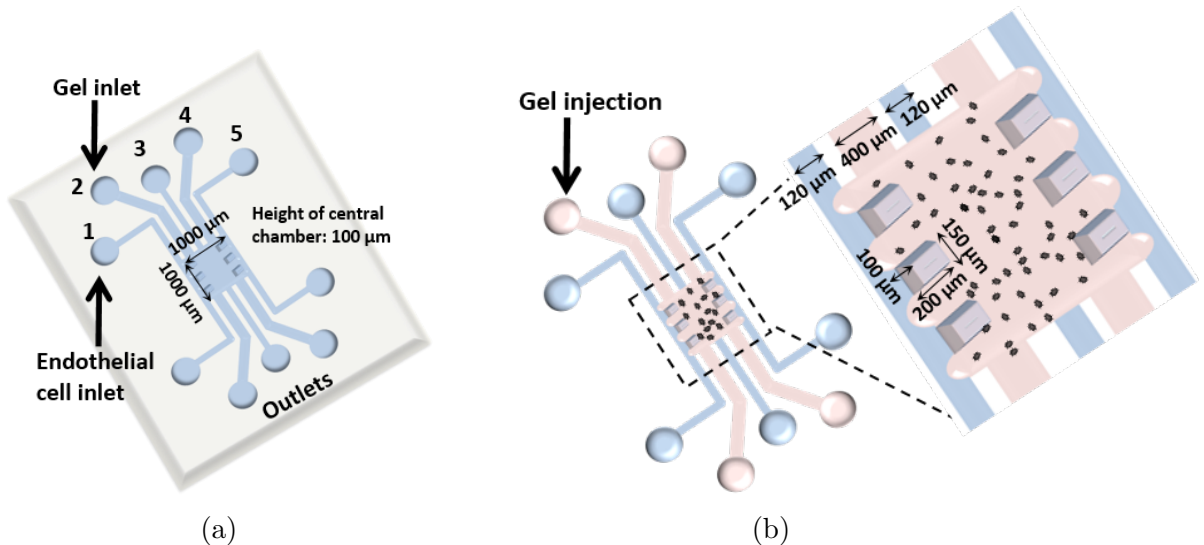


Figure 1: (a) Inlets 1 and 5 are used to supply a steady source of nutrients to the central compartment. Inlets 2-5 (and their corresponding outlets) are closed. (b) The central area consists of a 10% collagen 90% cell growth medium matrix, in which GBM cell lines can be seeded.

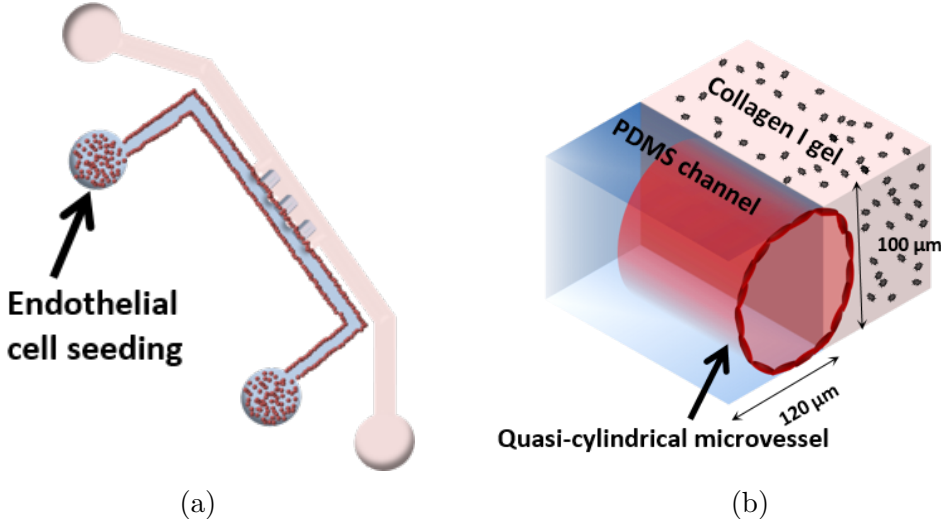


Figure 2: (a) Inlets 1 and 5 are seeded with endothelial cells. Ideally the rate of nutrient supply is large enough for a constant glucose and oxygen concentration to be maintained in the channel. (b) A blood vessel supply line is simulated as the endothelial cells cover the surfaces. We assume that there is little to no flow from the channel to the central region and that all supply is due to diffusion.

In order to model the OC effectively we must choose a geometry, BCs and ICs which are representative. Our region of interest is the central area where the GBM is growing, so we choose to model the geometry as that of a cuboid, figure 3.

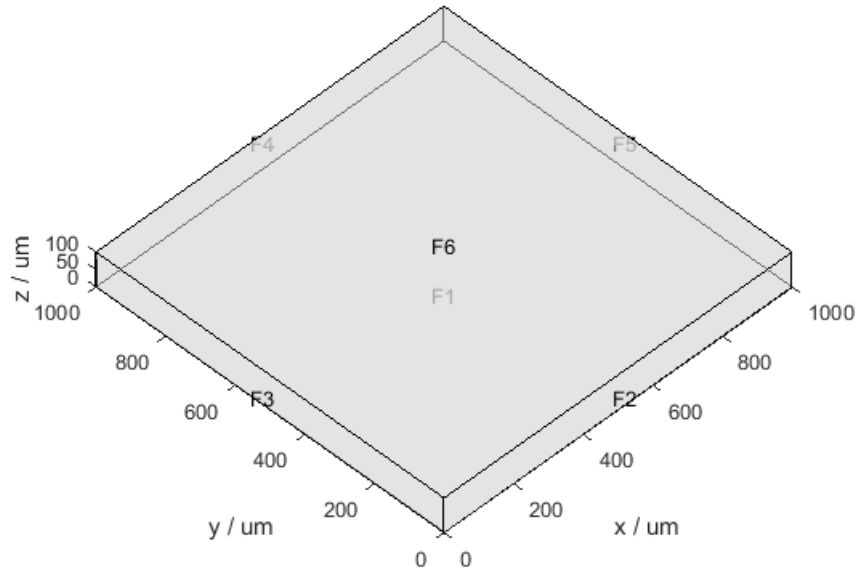


Figure 3: A simple cuboid captures the geometry of the situation, and we can model the supply of nutrients by applying choice boundary conditions to each of the surfaces. Here F3 and F5 represent the sides attached to the microvessels.

Our BCs are modelled as follows. On all faces we enforce the Neumann boundary condition  $\nabla u = 0$ , that is the flux of cells is zero as no cells can leave the region of interest. We enforce the same condition for any nutrient on faces where they are not entering, e.g. the flux of glucose is zero on all faces apart from F3 and F5. Supply of glucose and oxygen is modelled by enforcing Dirichlet boundary conditions on faces F3 and F5, where we set  $[O_2] = [O_2]_0$  and  $[g] = [g]_0$ . Here we must assume that there is no gradient in any nutrient along the microvessel, and that the supply of nutrients is fast enough to ensure that the BCs are truly constant. Likewise, we model diffusion of oxygen through the PDMS case as a Dirichlet boundary condition on F6, with the same value as the vessel (the diffusion of oxygen is so rapid, we assume that the concentrations equalise at the supplying faces as an approximation). We have no flux of oxygen in F1, F2, and F4; the base and top channels are closed.

The initial conditions of our problem are made using a set of Gaussian distributions whose centres are random. In our script, we use three in this way. Randomly distributed clusters of cells are simulated which result naturally from filling the central region with the cell-containing growth medium. Uniform initial conditions for oxygen and glucose are taken, the values being the same as the boundary conditions;  $[O_2](t = 0) = [O_2]_0$  and  $[g](t = 0) = [g]_0$ . One set of random centres was generated. These have been used throughout the investigation for consistency.

Face	Cancer	Oxygen	Glucose
F1	$\nabla u = 0$	$\nabla [O_2] = 0$	$\nabla [g] = 0$
F2	$\nabla u = 0$	$\nabla [O_2] = 0$	$\nabla [g] = 0$
F3	$\nabla u = 0$	$[O_2] = [O_2]_0$	$[g] = [g]_0$
F4	$\nabla u = 0$	$\nabla [O_2] = 0$	$\nabla [g] = 0$
F5	$\nabla u = 0$	$[O_2] = [O_2]_0$	$[g] = [g]_0$
F6	$\nabla u = 0$	$[O_2] = [O_2]_0$	$\nabla [g] = 0$

Table 1: Summary of boundary conditions. Unless explicitly stated,  $[O_2]_0 = 260\mu\text{mol}$  (estimated using Henry's Law and knowing that the partial pressure of oxygen in the side channel is 150mmHg) and  $[g]_0 = 5\text{mmol}$ .

### 3.2 Parameters

As has been discussed in section 2, our model depends on a number of parameters whose values can be estimated from the literature or experiment. Ultimately these parameters are unphysical, and we should see them as being values that we can adjust to fit observation. Table 2 contains a list of parameters and the values used. The diffusivities are those for water, as the growth matrix consists almost entirely of water; the collagen will not make an order of magnitude difference in the composite diffusivity.

Quantity	Value	Source	Notes
$D_c$	$100 \mu\text{m}^2 \text{d}^{-1}$		chosen to fit observed timescales
$\alpha$	$2 \text{ d}^{-1}$		chosen to fit observed timescales
$c_m$	$10^6 \text{ cm}^{-3}$	[7]	Value is approximate
$D_{o2}$	$8.64 \times 10^7 \mu\text{m}^2 \text{d}^{-1}$	[14]	
$k_{o2}$	$4.3 \mu\text{mol}$	[15]	Estimated using Henry's Law
$v_{o2}$	$100 \mu\text{mol d}^{-1}$	[15]	
$D_g$	$3.648 \times 10^6 \mu\text{m}^2 \text{d}^{-1}$	[16]	
$k_g$	$0.5 \text{ mmol}$	[6]	
$v_g$	$7 \text{ mmol d}^{-1}$	[6]	

Table 2: The parameters used in the main line of investigation. One day is 1d, and mol is short for moles per decimetre cubed.

The values of  $D_c$  and  $\alpha$  were given order of magnitude estimates as the literature gives a wide range of estimates which vary significantly depending on cell line used and method of estimation.

### 3.3 Numerical Scheme

We use PDE Toolbox in MATLAB [17] which consists of high-level tools for solving systems of PDEs using the finite element method (FEM) [18]. The basic operating principle of FEM is to fill a space of interest with a web of connected lines known as a mesh. Numerical integration is performed at the nodes (intersections of lines) where the solution estimates come from. All of this is handled automatically by MATLAB, and the only low-level parameter we specify is the maximal distance between the nodes. We are considering changes on a timescale of a few days, so the smallest natural length scale in our problem is  $2\sqrt{D_c t} \approx 40$ . By setting the maximal node spacing less than this (we chose 30) we should avoid spacial resolution errors. Temporal resolution is handled automatically by MATLAB which minimises an error function to beneath a pre-determined amount and adjusts the timesteps accordingly. The solution will fail if this tolerance limit is not met.

## 4 Results & Discussion

### 4.1 Organ-on-a-chip

Using the parameters found in 2, a simulation was run for a period of 51 days and the results are presented in figures 4, 5, and 6.

As can be seen in figure 4, the cancer evolves with approximate cylindrical symmetry from the centres of the core in 4a-4c. The cylindrical symmetry is expected given the order of magnitude difference in the vertical compared with the horizontal directions; the cancer grows and quickly reaches the top before it grows out toward the sides. One cluster of cells grows more rapidly than the other, which is the result of two of the three initial clusters being fairly close.

After a period of 21 days, 4d, the cancer has reached maximal concentration in most of the region. Despite  $u$  being very high, we do not see much cell death (for these parameters) and the low values of the Michaelis constants relative to the supplied nutrients ( $[g]_0/k_g = 10$ ,  $[O_2]_0/K_g = 60.5$ ) mean that the rates (equation 4) are close to their maximal values. Thus the maximum population remains close to one. When combined with the low nutrient gradients, seen in figures 5 and 6, this has the effect of making the maximal concentration throughout the region approximately one.

Some cell death is seen after 21 days as nutrient gradients, though small, are present. In the steady state, 4f, we see a pattern of cell death which causes the cell distribution to follow the nutrient distribution. There is a slightly higher concentration of nutrients toward the supply faces (see table 1) which results in a slightly higher maximal population.

These figures show that for natural estimates in the parameters, our model is qualitatively consistent with observation. However, high sensitivity to some parameters, discussed later, means the solution can vary significantly. While our model can capture the behaviour of the cancer growing in general, it is unlikely to be useful in predicting the development of a specific GBM OC.

Until comparisons are made with experimental data, we are limited in the conclusions we can draw. However, we can at least see that the steady state seems to be a uniform distribution. If the real distribution is not uniform, then this is either due to unmodelled effects (such as cell interaction), parameter variation, or our nutrition scheme being too simplistic.

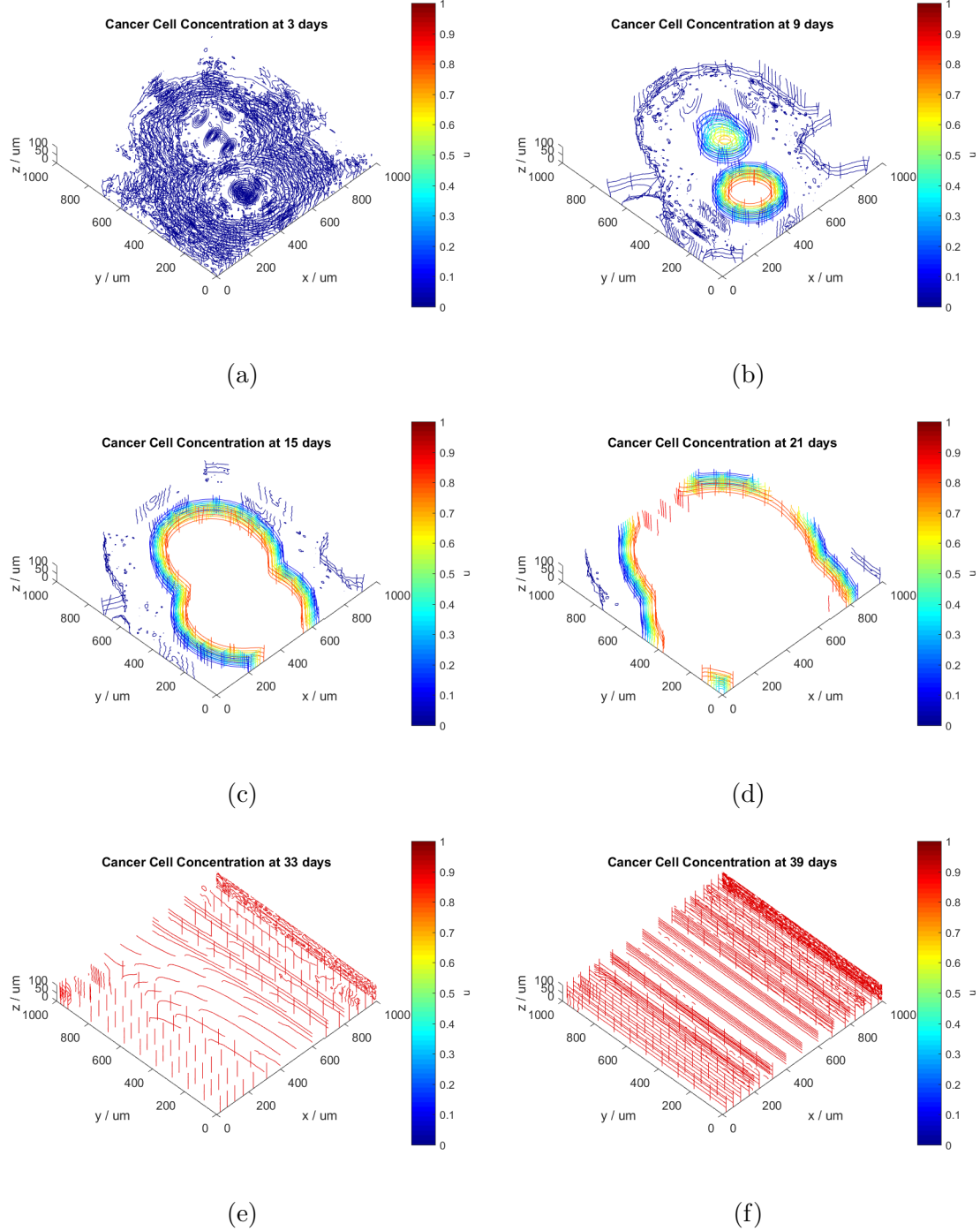


Figure 4: Cancer cell distribution as a function of space and time, for the conditions and parameters found in tables 1 and 2. Initial Gaussian centres are  $(553.7475, 578.2829, 39.4964)$ ,  $(597.1873, 640.3779, 65.8522)$ , and  $(415.7227, 253.0553, 43.7209)$ . By 39 days, the distribution has achieved a steady state.

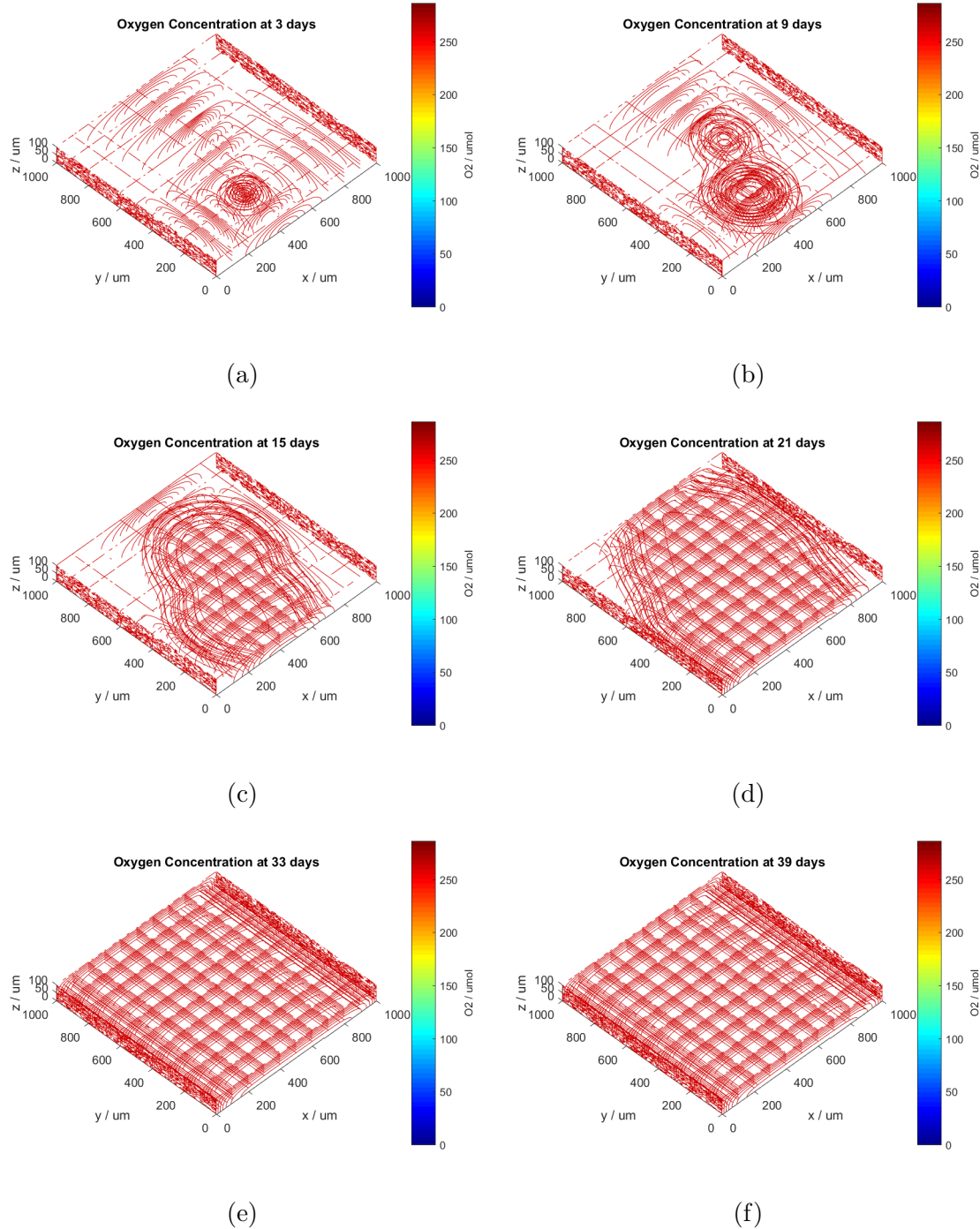


Figure 5: Oxygen concentration as a function of space and time for the cell distribution in figure 4. Although many contours which follow the form of  $u$  are displayed, the actual variation in  $[O_2]$  is very small.

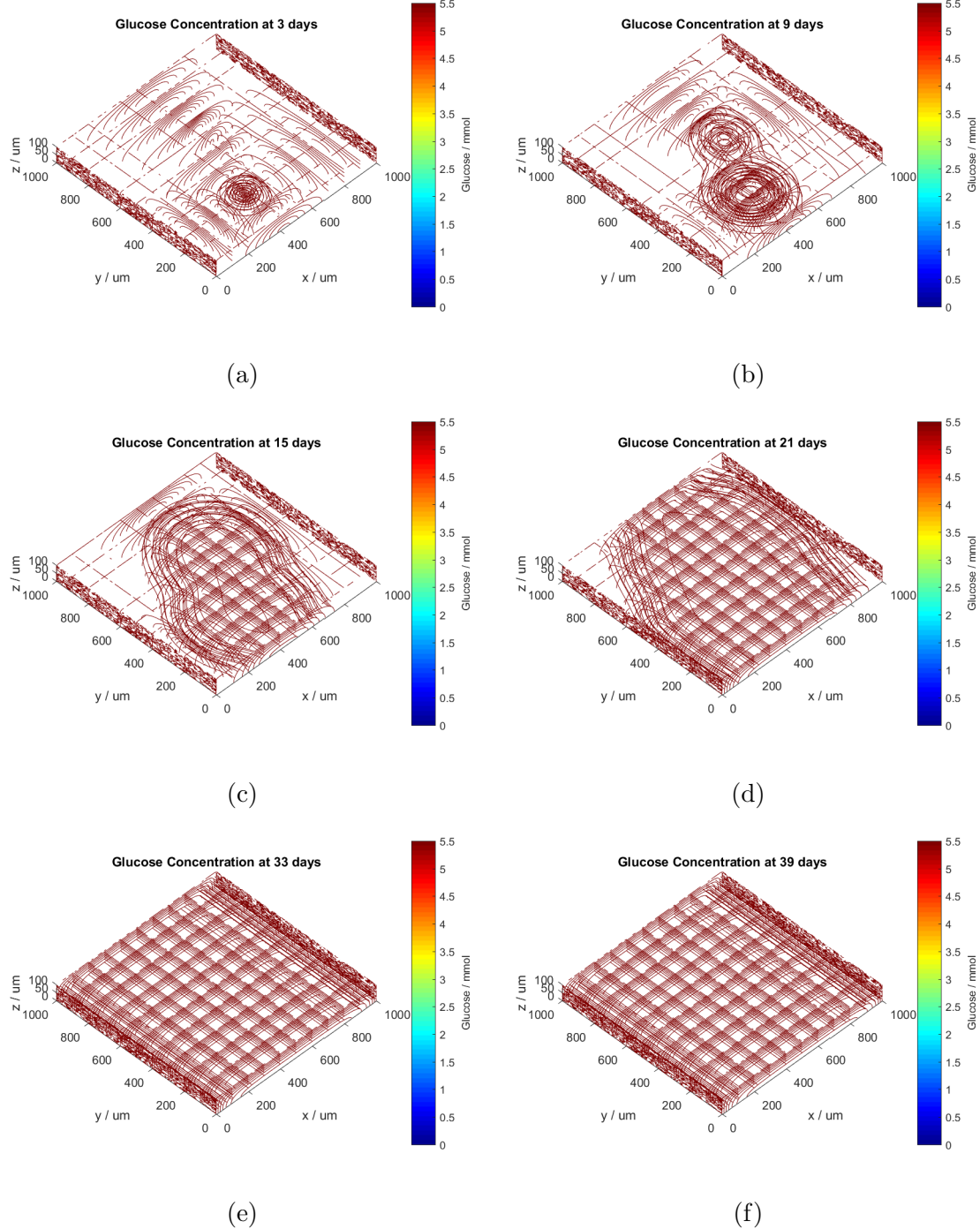


Figure 6: Glucose concentration as a function of space and time for the cell distribution in figure 4. Like  $[O_2]$ , actual variation in  $[g]$  is very small. The diffusion timescale (order of hours) is much smaller than the considered timescale, so the distribution is approximately constant.

## 4.2 Changing Glucose Supply

Now we investigate the effect of altering the glucose supply in the system. From figures 4 and 6, we see that a supply of  $[g]_0 = 5\text{mmol}$  is more than enough to support a maximal population, with very shallow gradients in the glucose distribution. We therefore investigate lower concentrations in the following subsections. Oxygen distributions have been omitted, as their gradients are minute and they have the same form as the glucose distributions.

Lowering  $[g]_0$  relative to  $k_g$  has two effects. Firstly, the maximal population falls in line with 3, since we have reduced the rate of metabolism by lessening the supply. Secondly, although the evolution of growth seems to posses the same symmetry as that in figure 6, the propagation of the tumour front is reduced in speed. This is qualitatively consistent with a travelling wave analysis of the logistic reaction-diffusion equation of cancer with no nutritional effects, which gives the tumour front speed as  $s \propto \sqrt{D_c \alpha}$  [19]. Since we effectively reduce alpha, equation 2, we reduce the tumour front velocity, which is consistent with the observation that lower nutrition leads to slower growth.

#### 4.2.1 1mmol

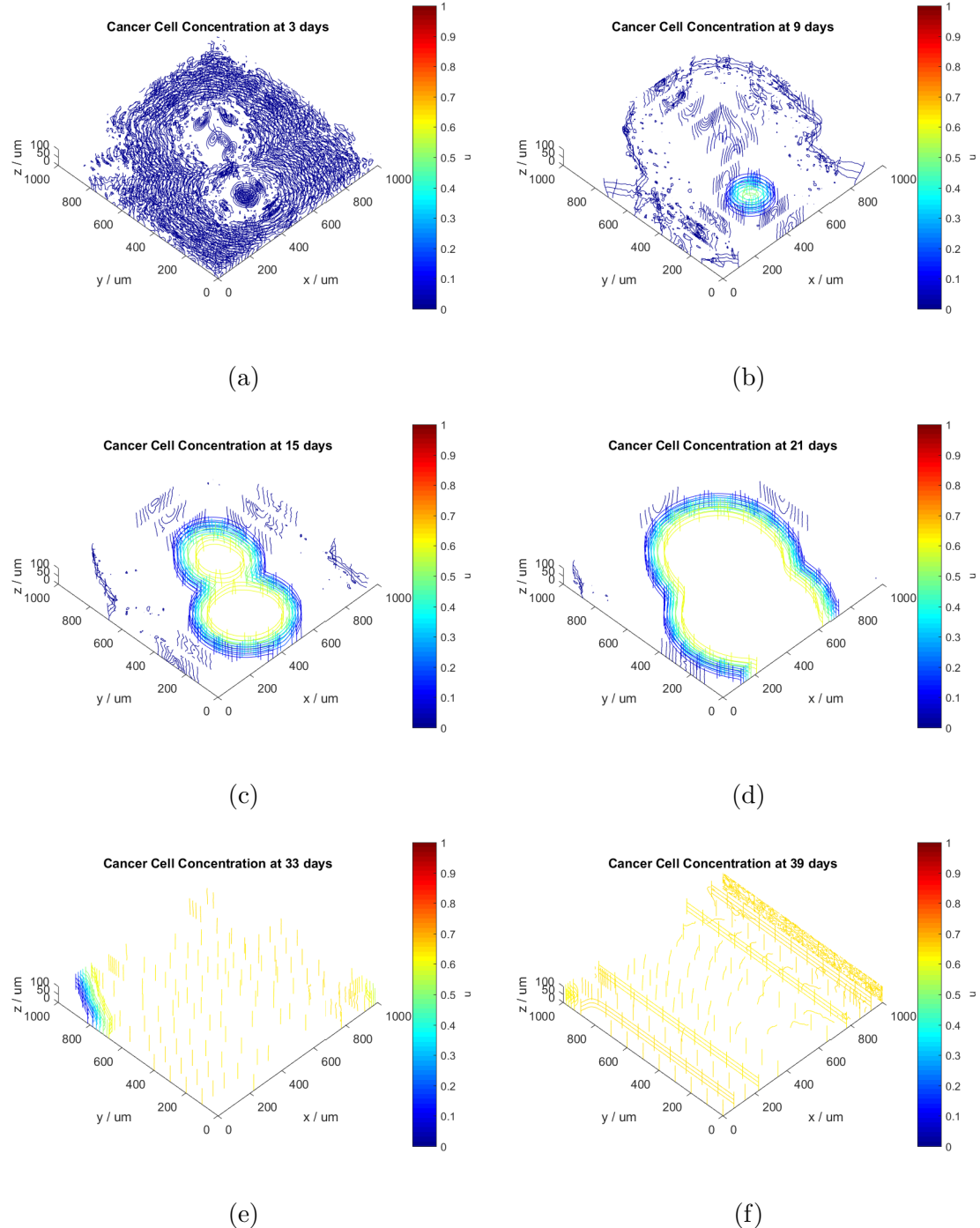


Figure 7: Cancer cell distribution as a function of space and time for the same parameters as in 4, save the change in  $[g]_0$ .

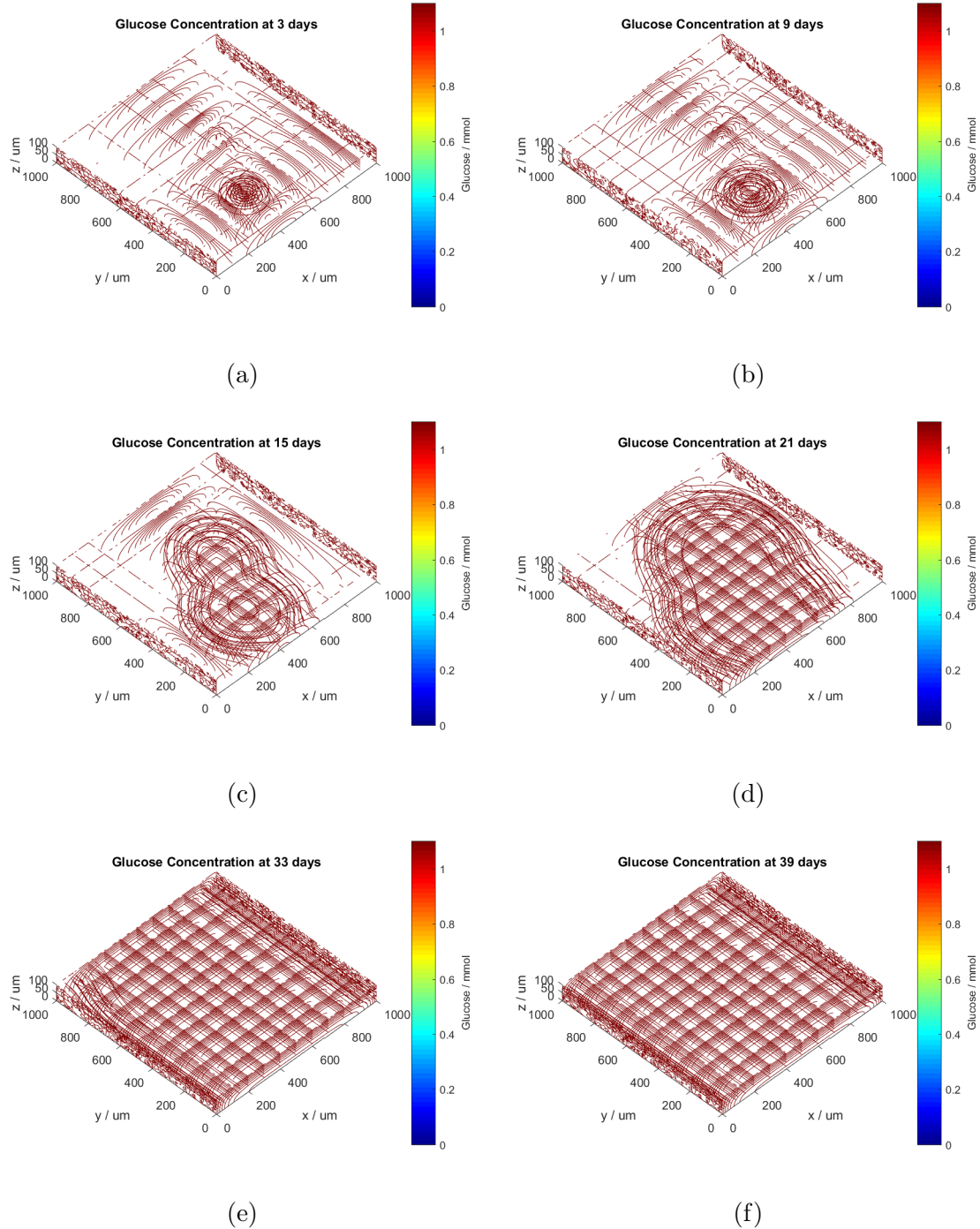


Figure 8: Glucose distribution as a function of space and time.  $v/v_m = 0.66$  throughout the region.

#### 4.2.2 0.5mmol

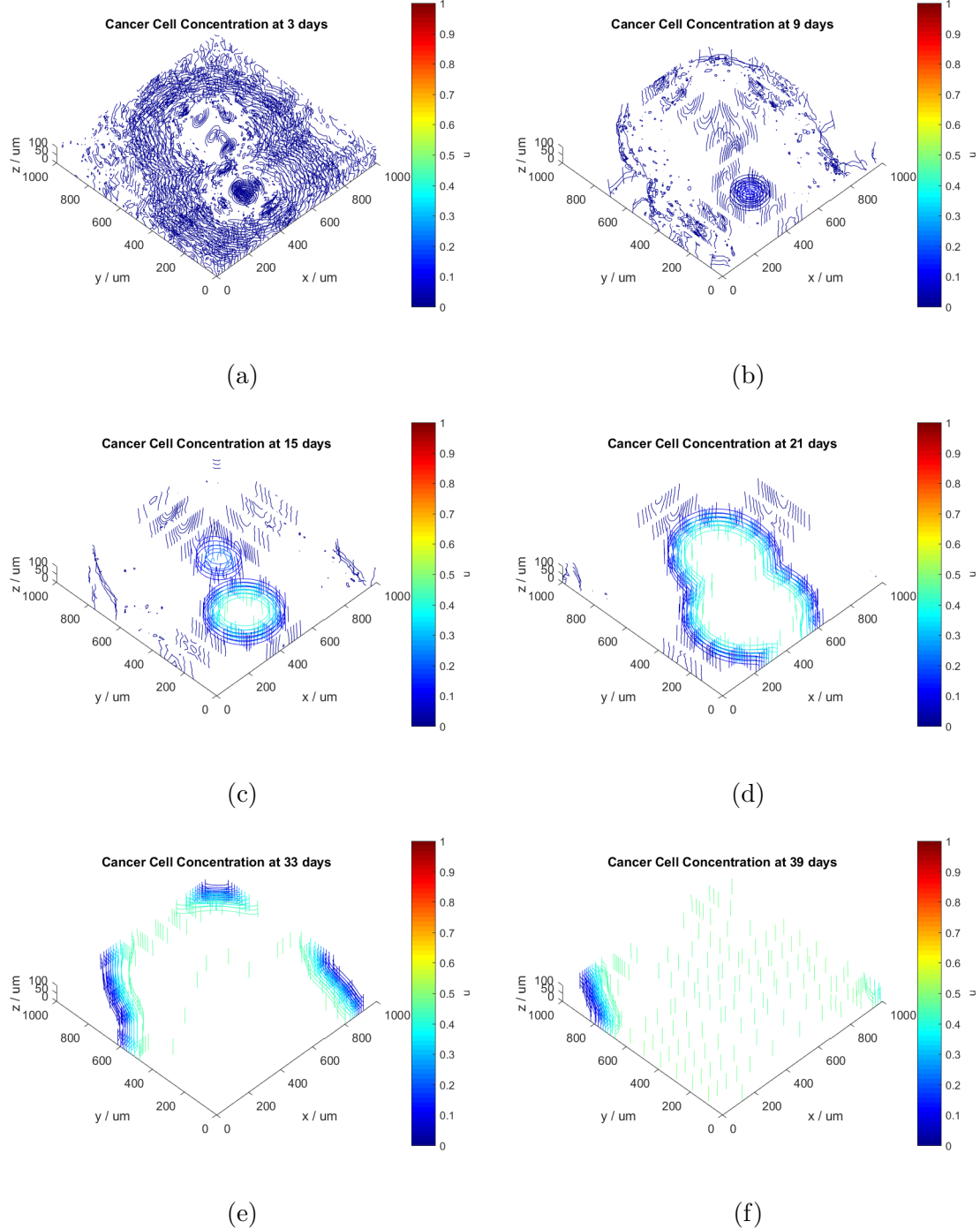


Figure 9: Cancer cell distribution as a function of space and time for the same parameters as in 4, save the change in  $[g]_0$ . The reduction in growth rate is clear by only 9 days (cf. (b) between figures).

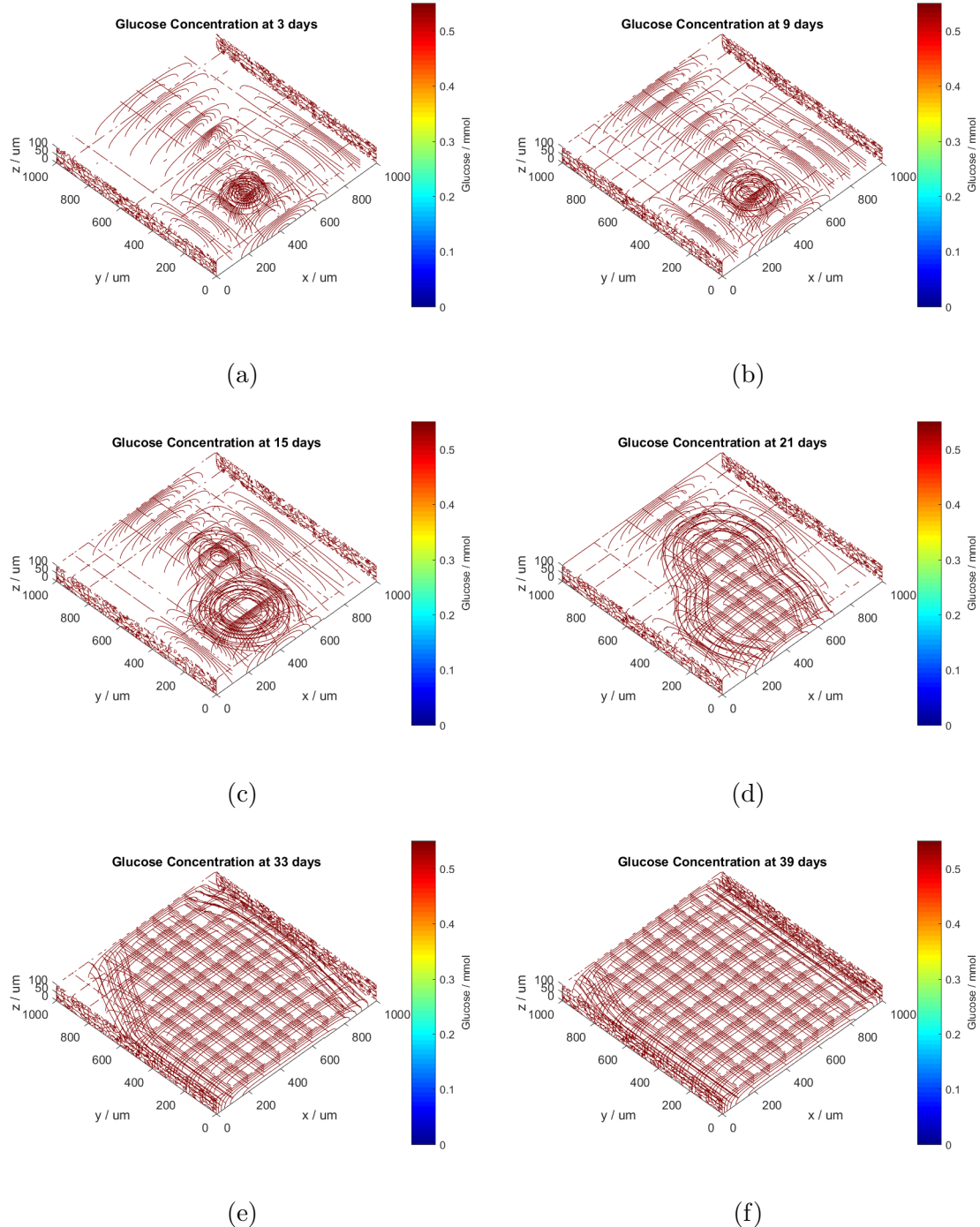


Figure 10: Glucose distribution as a function of space and time.  $v/v_m = 0.5$  throughout the region.

#### 4.2.3 0.1mmol

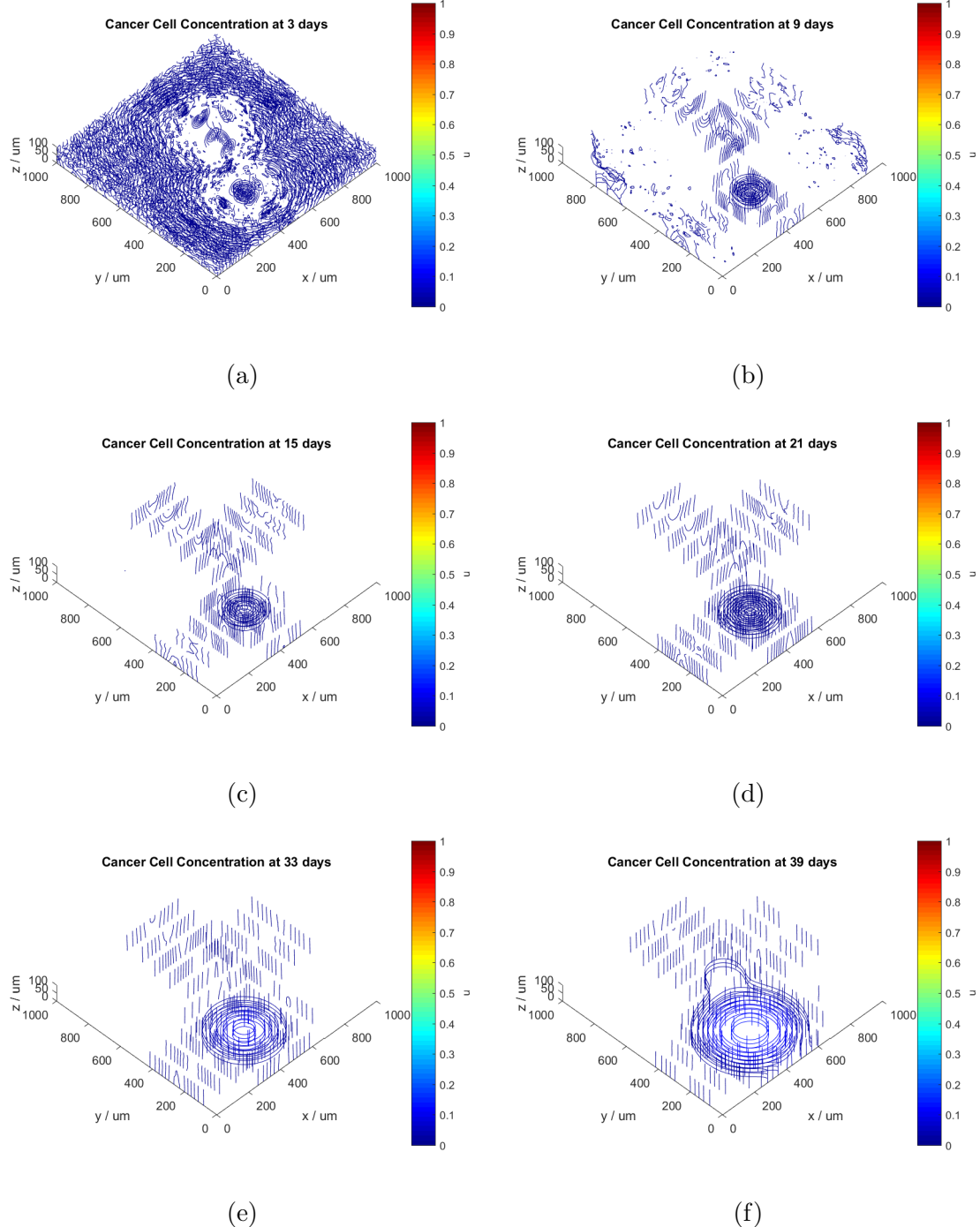


Figure 11: Cancer cell distribution as a function of space and time for the same parameters as in 4, save the change in  $[g]_0$ . Now the growth is significantly reduced, with the smaller cell cluster barely proliferating in this timescale.

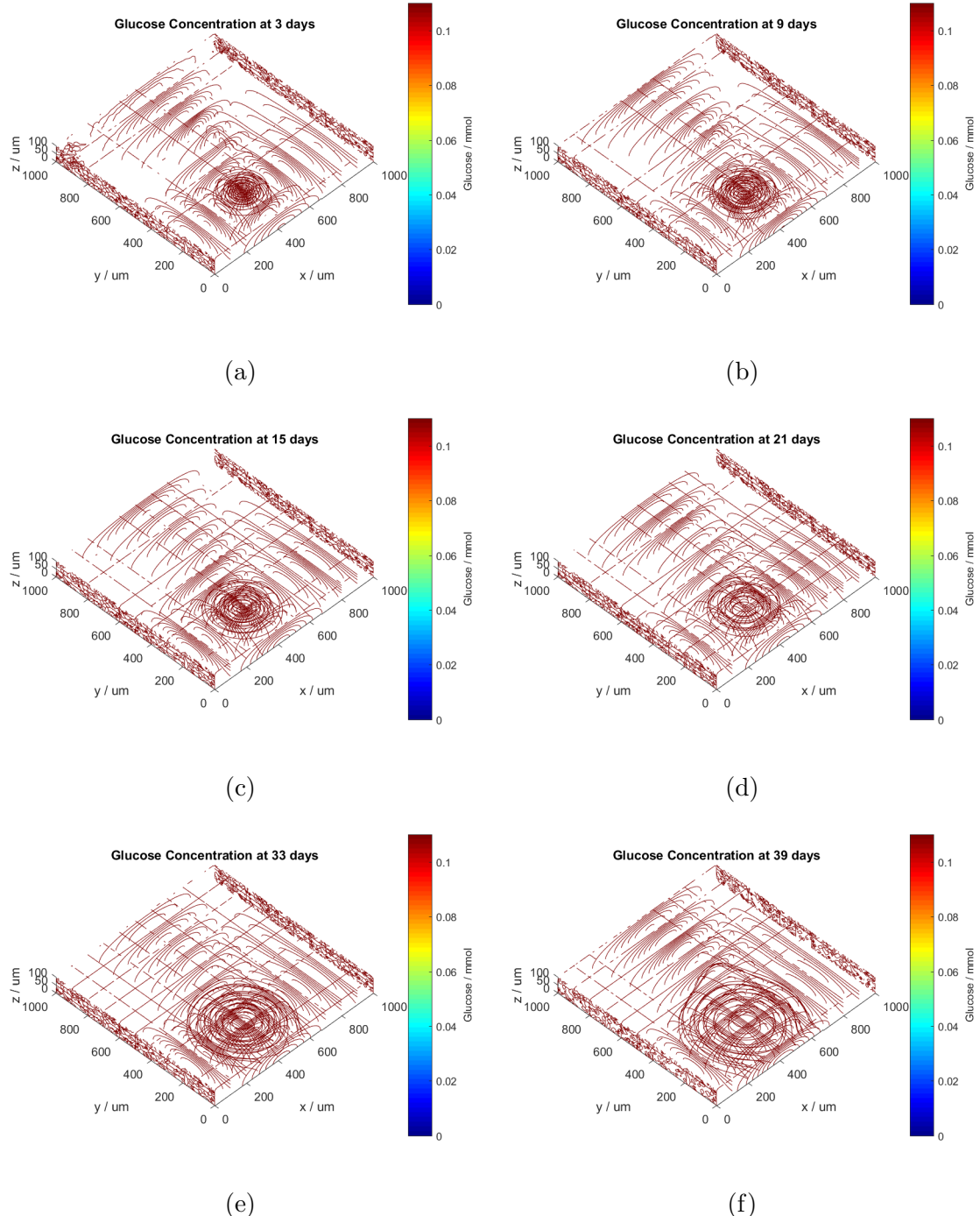


Figure 12: Glucose distribution as a function of space and time.  $v/v_m = 0.17$  throughout the region.

### 4.3 Model Sensitivity

Since all of the parameters presented in table 2 are accurate to within an order of magnitude only (or more in the case of  $D_c$ , which can be within  $[10^1, 10^4]$  in the tabled units), we tested the code by varying the parameters across orders of magnitude and displaying the cases where significant changes appear. For the sake of brevity and salience, only the cell distributions have been included in the figures.

Altering the cancer diffusivity, figure 13, seems to result in large-scale changes in growth. Firstly, the rapid spreading of cells results in a much wider distribution for low times (comparing figures 4b and 13c). The spreading is so great that the larger cell cluster seems to dominate the smaller cluster, whose only visible effect is to change the symmetry of the distribution late in the evolution.

The sensitivity to changes in nutrient diffusivity seems to be fairly low. Relative to the measured values, a decrease of two orders of magnitude in oxygen diffusivity does not seem to affect the solution significantly, figure 14. This makes sense given that the diffusion timescale is still small compared with the growth and nutrient consumption timescales ( $l^2/D \approx 10^{-2}d$  while  $\alpha^{-1} \approx 10^{-1}d$ ). A single order of magnitude reduction in glucose diffusivity has a similar result, but two orders of magnitude result in significant differences that can be seen in figure 15. Now the diffusion timescale is long enough for cell death to occur (as glucose falls in the centre of the cancer), and the steady state cell distribution shows a preference for the cells to grow near the glucose supply. However, variations in the diffusivity are unlikely to be this order magnitude. Increasing the diffusivities results in no changes from figure 4, again due to the low diffusion timescale.

Like the variation in glucose supply, the system seems to be very sensitive to changes in the Michaelis constants, figures 16 and 17. These order of magnitude increases cause significant reductions in cancer front propagation and maximal population (which is consistent with 5). Since in both cases the diffusivities are still very high, the concentrations of glucose and oxygen remain approximately constant throughout the region. So we have:

$$\frac{v}{v_m} \approx \frac{[O_2]_0}{k_{o2} + [O_2]_0},$$

and the equivalent for glucose. Since these changes make the constant a similar order of magnitude as the supplied nutrient, and this function changes most rapidly in  $k$  when it is less than the nutrient concentration, our model is sensitively dependent on these parameters (see equations 2 and 3).

Changing the maximal rates seems to have little to no effect. The reason for this is that the diffusivities are so large at this lengthscale that any gradient created by consumption is corrected by diffusion. Consider the dimensionless variable:

$$X = \frac{l^2 v_m}{[n]_0 D},$$

where  $[n]_0$  is some nutrient supply value,  $D$  is its diffusivity,  $l$  is a typical system lengthscale, and  $v_m$  is the maximum consumption rate.  $X$  is a measure of the relative strength of consumption to diffusion. In order to get  $X \approx 1$ , i.e. consumption and diffusion are comparable, we would have to increase  $v_{o2}$  by three orders of magnitude, or  $v_g$  by two. In figures 4, 18, and 19 we have  $X \ll 1$  so, given nothing else has changed, they look very similar.

### 4.3.1 Diffusivity

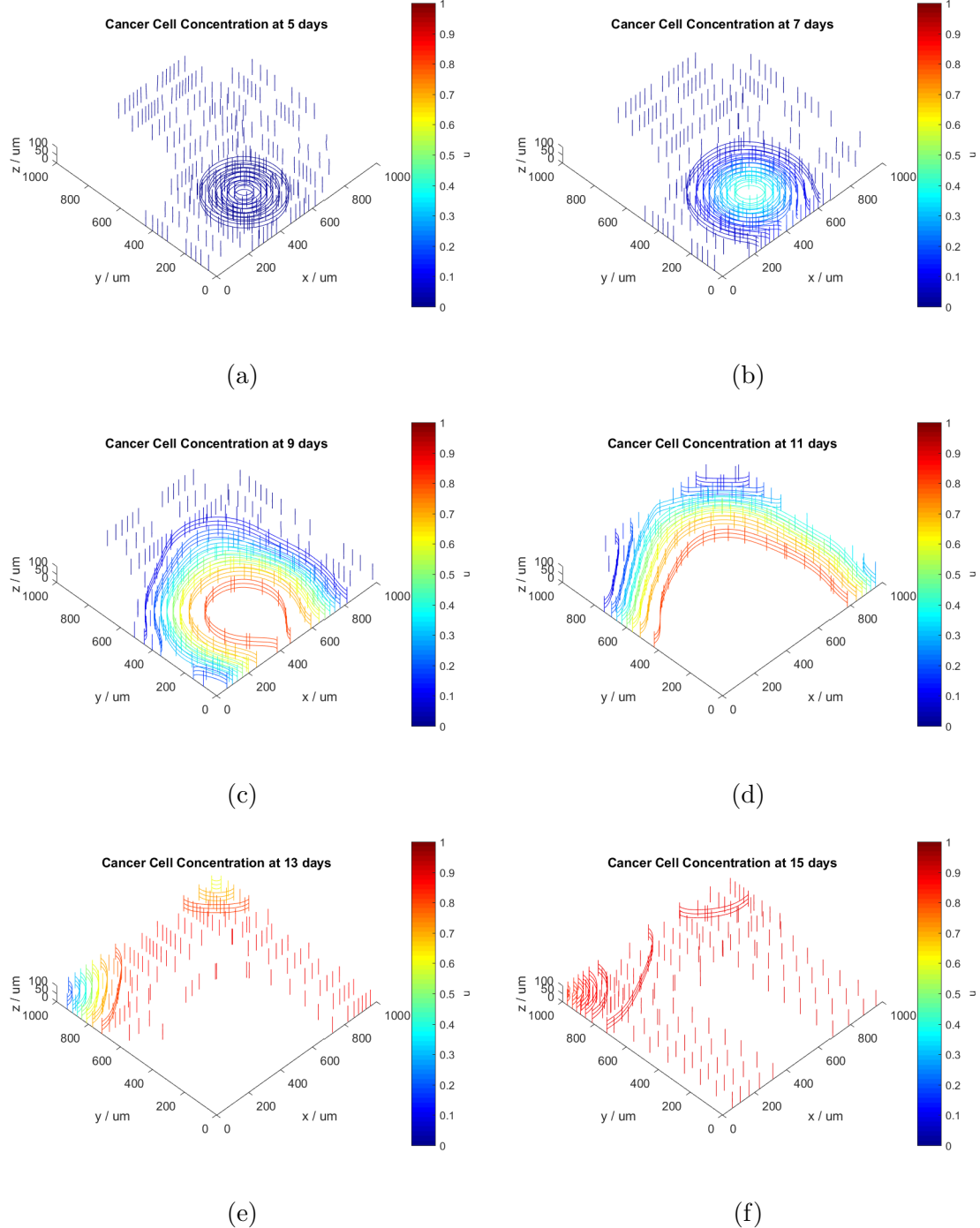


Figure 13: Setting  $D_c = 1000 \mu\text{m}^2 \text{d}^{-1}$  results in more rapid growth, cf. figure 4. The high diffusivity leads to spreading of the initial clusters, which in the case of the smaller one has led to it almost disappearing.

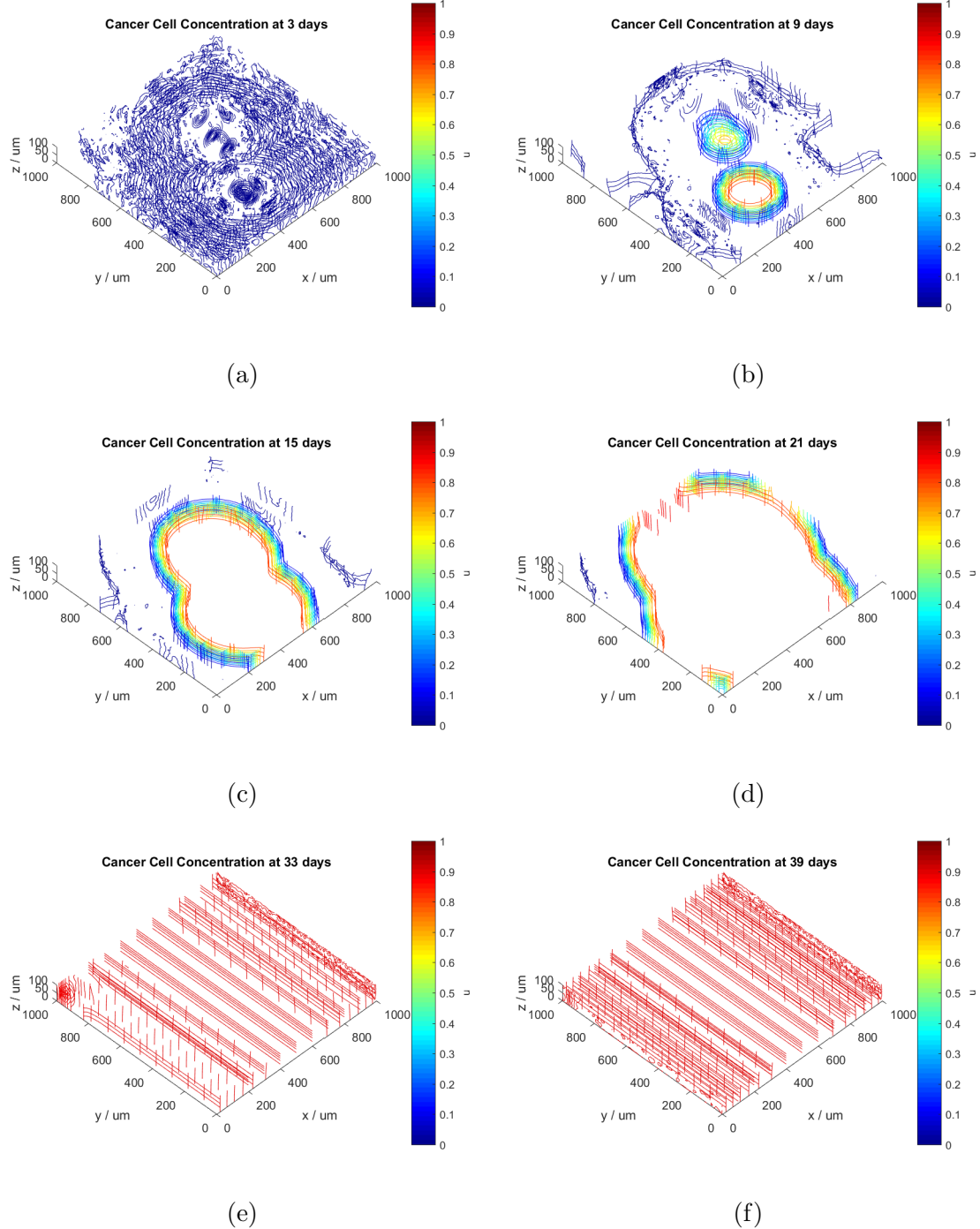


Figure 14: Here the oxygen diffusivity was reduced by two orders of magnitude to  $8.64 \times 10^5 \mu\text{m}^2 \text{d}^{-1}$ , far outside its natural range. Comparison with figure 6 shows few differences.

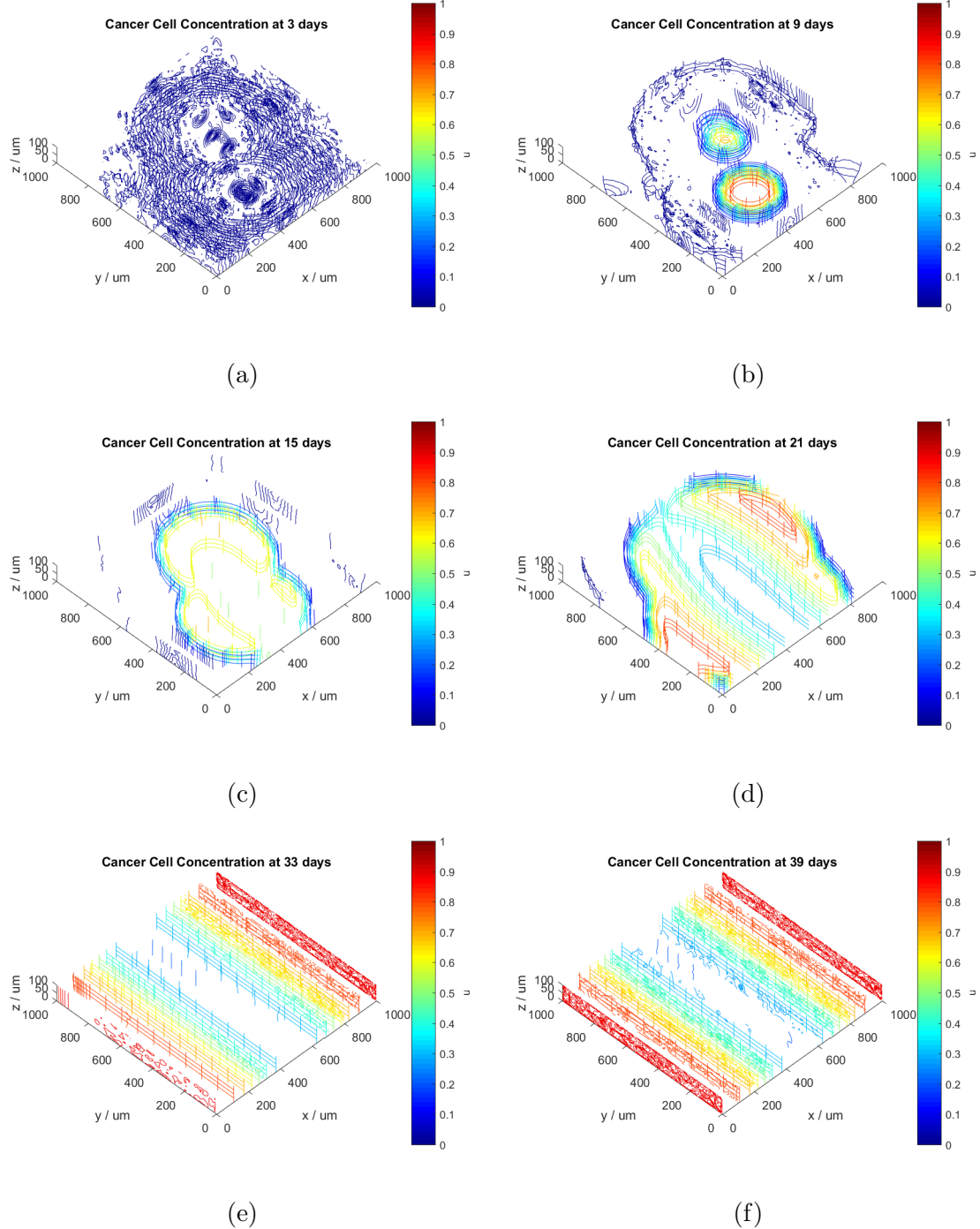


Figure 15: Reducing the glucose diffusivity by two orders of magnitude ( $D_g = 3.648 \times 10^4 \mu\text{m}^2 \text{d}^{-1}$ ). The steady state distribution in f is now radically different from figure 6f.

### 4.3.2 Michaelis Constant

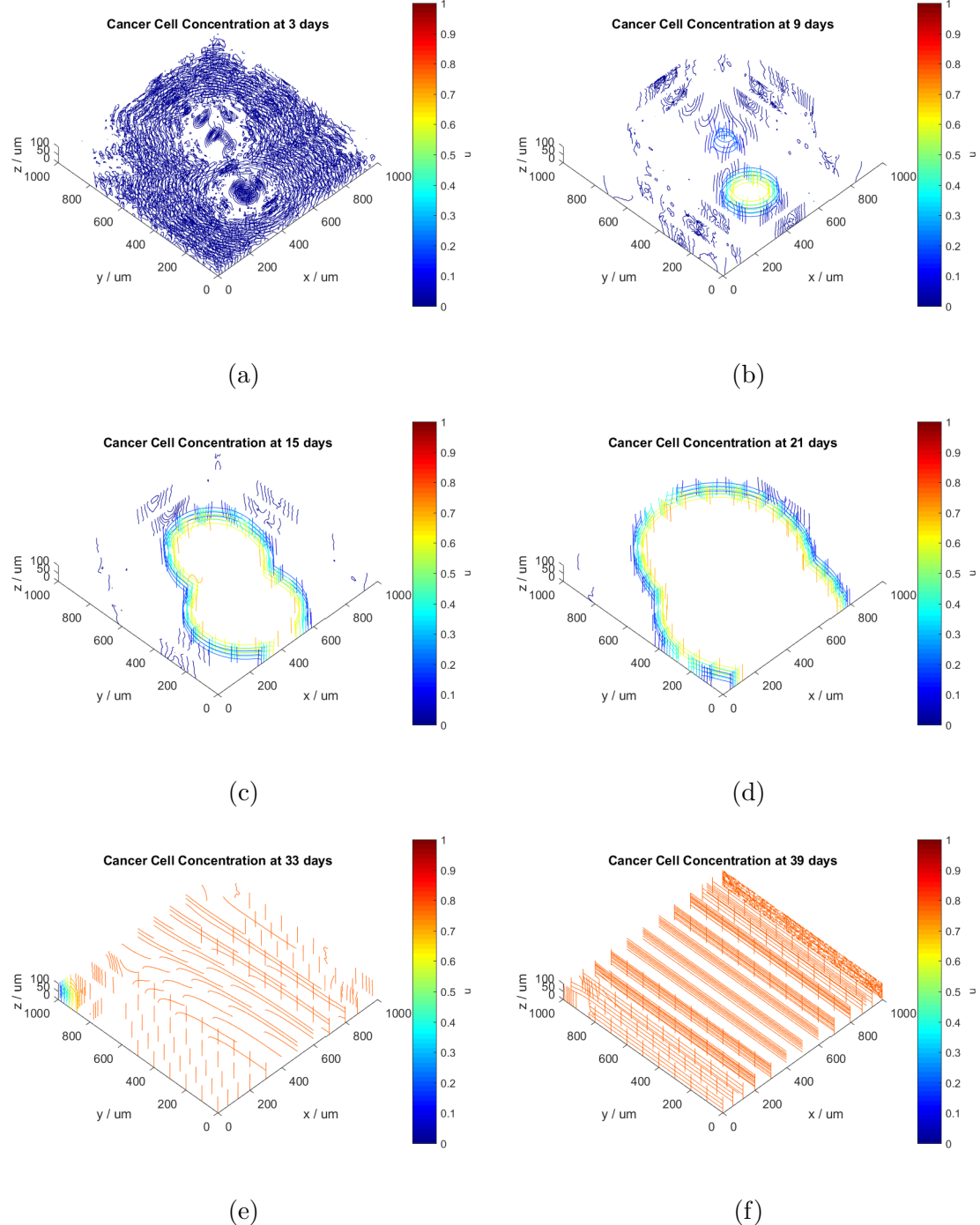


Figure 16: We increase the Michaelis constant for oxygen by an order of magnitude (to  $43\mu\text{mol}$ ). The broad evolution of the cancer has not changed much in timescale or form. However, the reduction in rate is significant enough to affect the maximum population.

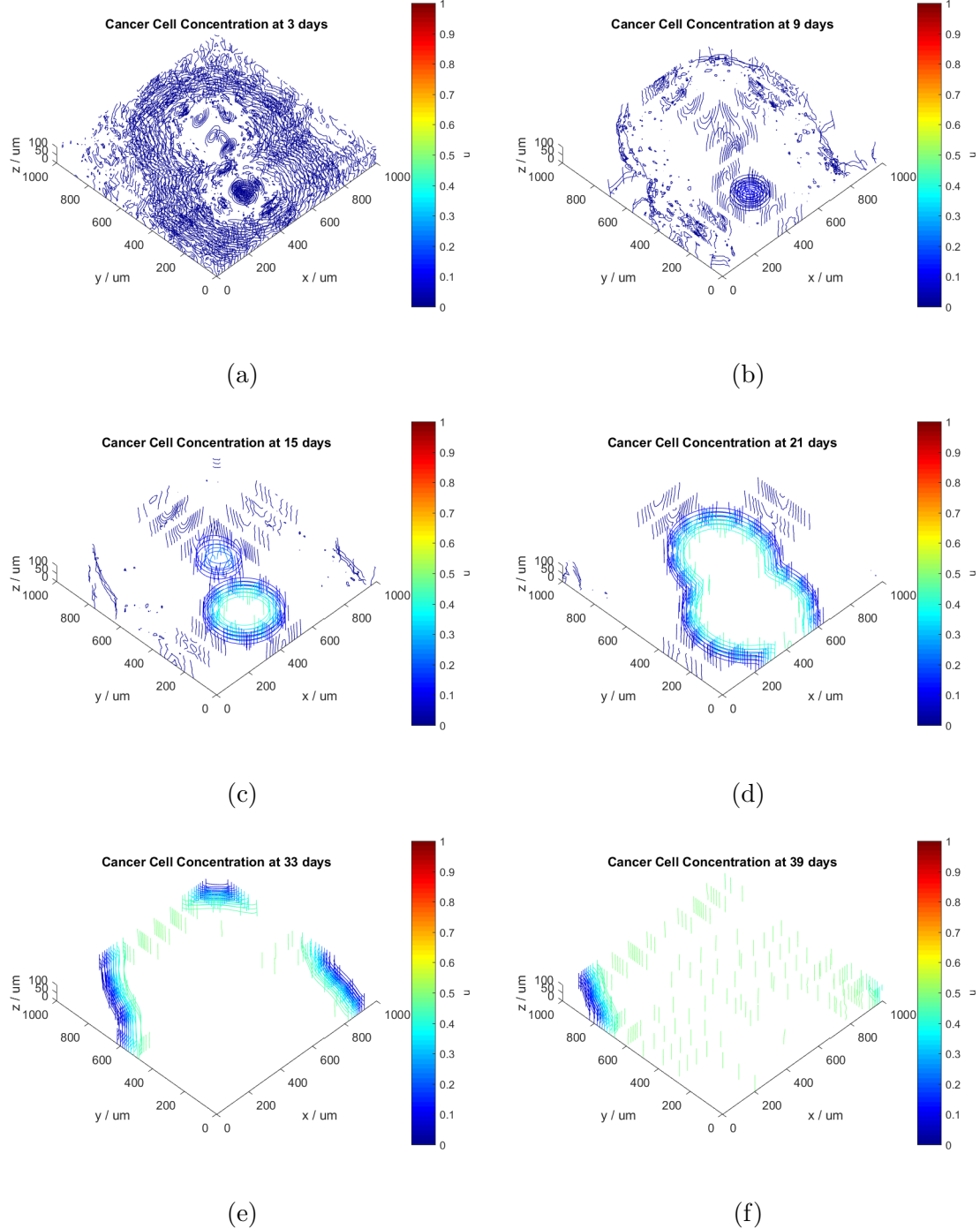


Figure 17: When we set  $k_g = 5\text{mmol}$ , there is a significant loss in growth rate and reduction in maximum population. This is expected as the Michaelis constant is now equal to the steady state glucose concentration.

## 4.4 Maximal Rates

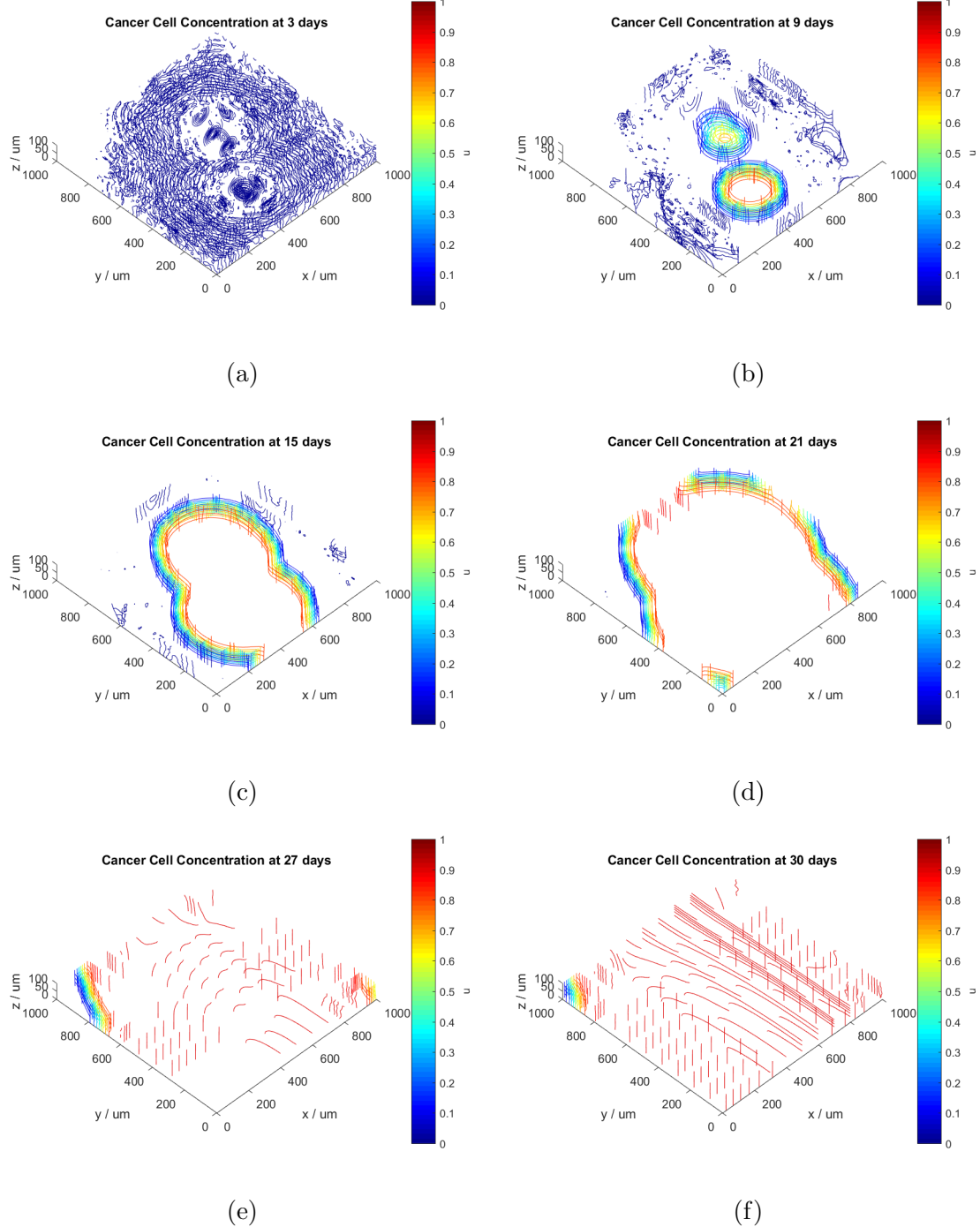


Figure 18: Here we raise  $v_{o2}$  by an order of magnitude, to  $1000 \mu\text{mol d}^{-1}$ , with little change from figures 4 and 19.

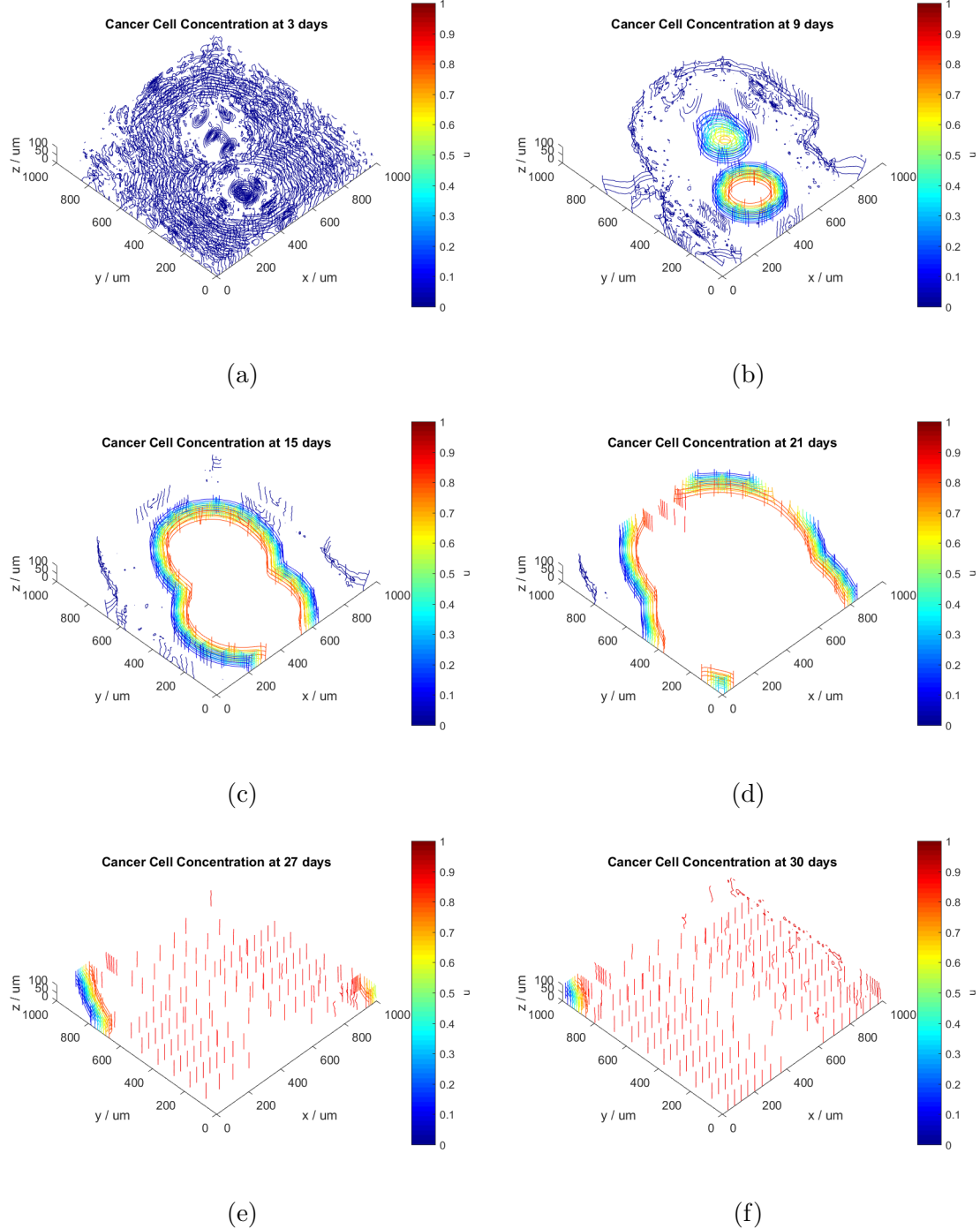


Figure 19: Here we raise  $v_g$  by an order of magnitude, to  $70\text{mmol d}^{-1}$ , with little change from figures 4 and 18.

## 4.5 The 2mm Rule

In real tumours, angiogenesis is observed when nutrient diffusion becomes a limiting factor for growth [20]. An oft quoted rule is that this becomes necessary when the tumour diameter becomes 1 – 2mm in size [21]. This is roughly the lengthscale of oxygen (and other nutrient) diffusion on the timescale of tumour evolution. Here we attempt to test this using our model to replicate *in vivo* conditions. In this case our basic geometry is altered to a greater scale, a 4 by 4 by 10mm cuboid. Using the same face convention as figure 3, we have set  $[O_2] = 83.4\mu\text{mol}$  on F3 and  $[O_2] = 51.2\mu\text{mol}$  on F5. This is intended to simulate the difference between arterial and venous blood oxygen concentrations [22]. We have also set  $\nabla[O_2] = 0$  on F6, as we no longer have PDMS diffusion. Side concentrations of glucose are the same, as arterial and venous glucose levels do not differ significantly *in vivo* [23]. The remaining BCs are identical to 1, and the parameters are the same as 2 (rescaled to mm lengthscales, and the upper limit on  $D_c = 0.01\text{mm}^2\text{d}^{-1}$  has been taken to produce evolution on a manageable timescale).

From the plots in figure 20, we can see that when the tumour reaches roughly 2mm in size there is cell death. As the tumour grows, central cell death continues. This is supportive of the 2mm rule, since at this point real tumour would have to become vascular if significant necrosis is to be prevented. Although this model is flawed in that transfer of nutrients is entirely diffusive between millimetre-sized blood vessels, it does at least recover an observed behaviour of real cancers which grow in similar oxygenation gradients. As an aside, we note that  $X \approx 10^1$ , which results in a non-uniform cell distribution in the steady state.

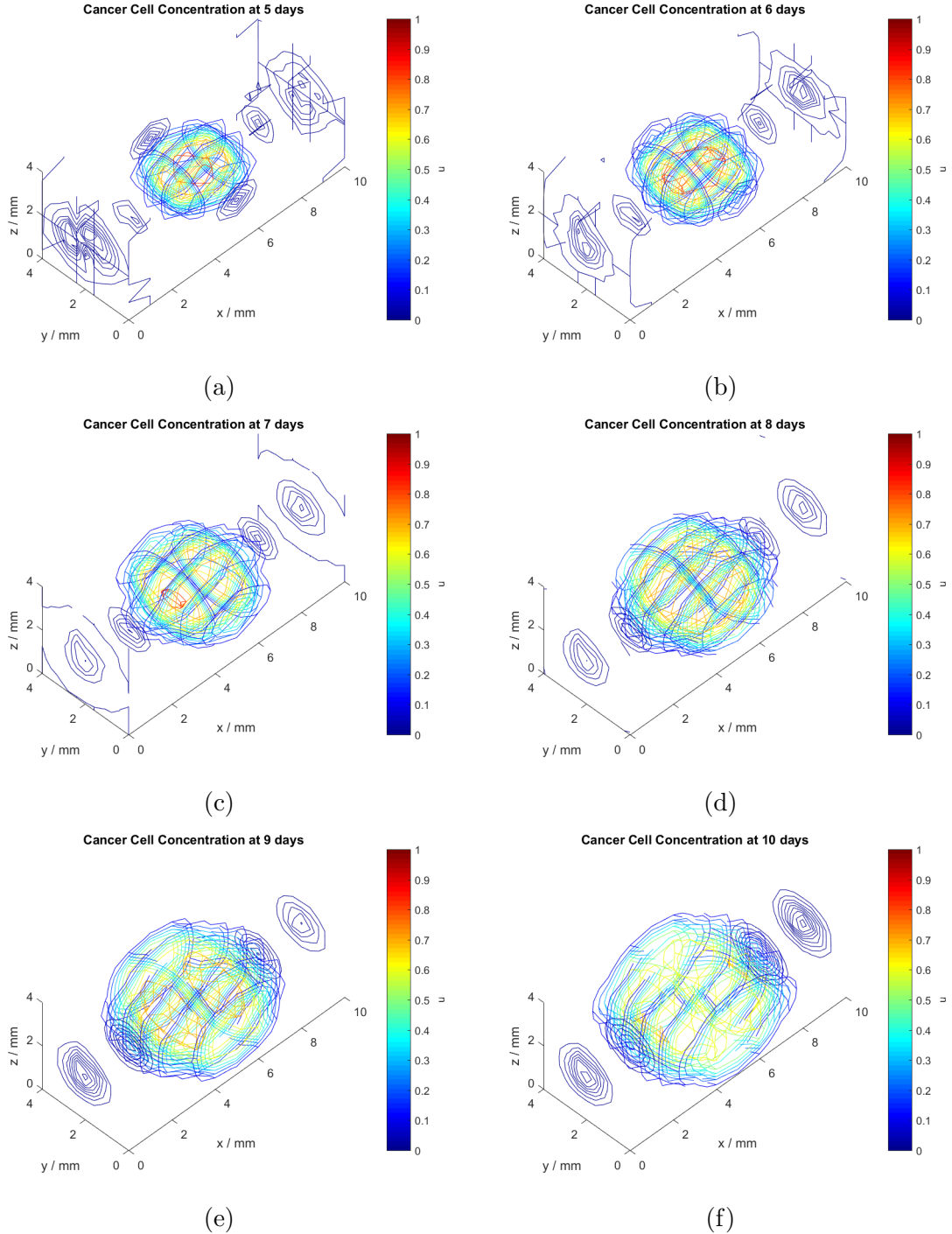


Figure 20: Evolution of the modelled tumour, a Gaussian initial condition is used with maximal initial concentration and standard deviation of 0.3mm. From (b) to (d) the loss in red at the centre is indicative of cell death. Note that the tumour is roughly 2mm in diameter when this occurs. Occurrence of cell death is clear by (e) and (f), as the central cell concentration is no longer the highest cell concentration.

## 5 Conclusion

By implementing a reaction-diffusion model of cancer growth, including oxygen and glucose limited growth, we have created a simulation which is qualitatively consistent with observed behaviours for GBM growing in an OC. A uniform distribution in the steady state is predicted.

The simulation is sensitively dependent on the Michaelis constants, but insensitive to changes in the reaction rates to within two orders of magnitude. Similarly, sensitivity to diffusivity changes is low for the nutrients, but significant for the cells.

We have also applied the same theory to a simple *in vivo* model of a small GBM tumour. The growth of this tumour displayed quantitative consistency, to within a millimetre, of the 2mm angiogenesis rule in clinical oncology.

## 6 References

- [1] Patil et al. Prognosis of patients with multifocal glioblastoma: a case-control study. *Journal of Neurosurgery*, 117(4):705–711, 2012. PMID: 22920963.
- [2] Tiina Roose, S. Jonathan Chapman, and Philip K. Maini. Mathematical models of avascular tumor growth. *SIAM Review*, 49(2):179–208, 2007.
- [3] Haralampos Hatzikirou, Andreas Deutsch, Carlo Schaller, Matthias Simon, and Kristin Swanson. Mathematical modelling of glioblastoma tumour development: A review. *Mathematical Models and Methods in Applied Sciences*, 15(11):1779–1794, 11 2005.
- [4] Kristin R. Swanson, Carly Bridge, J.D. Murray, and Ellsworth C. Alvord Jr. Virtual and real brain tumors: using mathematical modeling to quantify glioma growth and invasion. *Journal of the Neurological Sciences*, 216(1):1 – 10, 2003.
- [5] Jessica B. McGillen, Catherine J. Kelly, Alicia Martnez-Gonzlez, Natasha K. Martin, Eamonn A. Gaffney, Philip K. Maini, and Vctor M. Prez-Garca. Glucose-lactate metabolic cooperation in cancer: Insights from a spatial mathematical model and implications for targeted therapy. *Journal of Theoretical Biology*, 361:190 – 203, 2014.
- [6] Berta Mendoza-Juez, Alicia Martínez-González, Gabriel F. Calvo, and Víctor M. Pérez-García. A mathematical model for the glucose-lactate metabolism of in vitro cancer cells. *Bulletin of Mathematical Biology*, 74(5):1125–1142, 2012.
- [7] R Rockne, J K Rockhill, M Mrugala, A M Spence, I Kalet, K Hendrickson, A Lai, T Cloughesy, E C Alvord Jr, and K R Swanson. Predicting the efficacy of radiotherapy in individual glioblastoma patients *in vivo*: a mathematical modeling approach. *Physics in Medicine and Biology*, 55(12):3271, 2010.
- [8] Kansal et al. Simulated brain tumor growth dynamics using a three-dimensional cellular automaton. *Journal of Theoretical Biology*, 203(4):367 – 382, 2000.

- [9] Sangeeta N. Bhatia and Donald E. Ingber. Microfluidic organs-on-chips. *Nat Biotech*, 32(8):760–772, Aug 2014.
- [10] Yuan Xie et al. The human glioblastoma cell culture resource: Validated cell models representing all molecular subtypes. *EBioMedicine*, 2(10):1351 – 1363, 2015.
- [11] E.O. Alzahrani, Asim Asiri, M.M. El-Dessoky, and Y. Kuang. Quiescence as an explanation of gompertzian tumor growth revisited. *Mathematical Biosciences*, 254:76 – 82, 2014.
- [12] Jeremy M. Berg, John L. Tymoczko, Gergory J. Gatto, and Lubert Stryer. *Biochemistry*. W.H. Freeman & Company, 2015.
- [13] M. V. Liberti and J. W. Locasale. The Warburg Effect: How Does it Benefit Cancer Cells? *Trends Biochem. Sci.*, 41(3):211–218, Mar 2016.
- [14] A. Martinez-Gonzalez, G. F. Calvo, L. A. Perez Romasanta, and V. M. Perez-Garcia. Hypoxic cell waves around necrotic cores in glioblastoma: a biomathematical model and its therapeutic implications. *Bull. Math. Biol.*, 74(12):2875–2896, Dec 2012.
- [15] Alexandru Dau, Iuliana Toma-Dau, and Mikael Karlsson. Theoretical simulation of tumour oxygenation and results from acute and chronic hypoxia. *Physics in Medicine and Biology*, 48(17):2829, 2003.
- [16] Yi Jiang, Jelena Pjesivac-Grbovic, Charles Cantrell, and James P. Freyer. A multiscale model for avascular tumor growth. *Biophysical Journal*, 89(6):3884 – 3894, 2005.
- [17] Matlab. PDE Toolbox R2016b. <https://www.mathworks.com/products/pde.html>.
- [18] Robert D. Cook, David S. Malkus, and Michael E. Plesha. *Concpts and Applications of Finite Element Analysis*. John Wiely & Sons, 1989.
- [19] Philip Gerlee and Sven Nelander. Travelling wave analysis of a mathematical model of glioblastoma growth. *Mathematical Biosciences*, 276:75 – 81, 2016.
- [20] Lucia Ricci-Vitiani, Roberto Pallini, Mauro Biffoni, Matilde Todaro, Gloria Invernici, Tonia Cenci, Giulio Maira, Eugenio Agostino Parati, Giorgio Stassi, Luigi Maria Larocca, and Ruggero De Maria. Tumour vascularization via endothelial differentiation of glioblastoma stem-like cells. *Nature*, 468(7325):824–828, Dec 2010.
- [21] Femke Hillen and Arjan W. Griffioen. Tumour vascularization: sprouting angiogenesis and beyond. *Cancer Metastasis Rev*, 26(3-4):489–502, Dec 2007. 9094[PII].
- [22] Lauralee Sherwood. *Human Physiology: From Cells to Systems*. Cengage Learning, 2013.
- [23] Ahmad Yaraghi, Nastaran Eizadi Mood, and Leila Kamali Dolatabadi. Comparison of capillary and venous blood glucose levels using glucometer and laboratory blood glucose level in poisoned patients being in coma. *Adv Biomed Res*, 4:247, Nov 2015. ABR-4-247[PII].

## 7 Acknowledgements

I would like to thank Dr Shery Huang for supervising this project, and the other members of her ‘Biointerface’ group for their assistance. In particular I would like to thank Magda Gerigk whose experimental work on the glioblastoma on a chip was essential to the motivation and completion of this project. The images in figures 1 and 2 were also supplied by Magda.

## 8 Appendix

### 8.1 Code

This listing contains code that was used for all parts of the investigation apart from the 2mm rule section. That code has been submitted electronically, but does not differ too significantly from this script.

```
1 %This script implements the reaction-diffusion model of cancer using the
2 %finite element modelling methods in PDE toolbox.
3 %
4 %The system being modelled is that of an organ-on-a-chip and a cuboidal
5 %geometry has been chosen to model the system with appropriate boundary
6 %conditions
7 %
8
9 clear variables
10 %
11 %Parameters
12 global D_c
13 global D_O2
14 global D_g
15 global alpha
16 global K_o2
17 global v_o2
18 global O2_0
19 global K_g
20 global v_g
21 global g_0
22
23 %this will print the values to the console
24 %default
25 D_c = 100 %um^2/day (can be up to 2000) %100
26 D_O2 = 8.64e7 %um^2/day %8.64e7
27 D_g = 3.648e6 %um^2/day %3.648e6
28 alpha = 0.2 %per day %2
29 K_o2 = 4.3 %umol %4.3
30 v_o2 = 100 %umol/day %100
31 O2_0 = 260 %umol %260
32 K_g = 0.5 %mmol %0.5
33 v_g = 700 %mmol/day %7
34 g_0 = 5 %mmol %5
35 c_coeffs = [D_c;0;0;0;D_c;0;0;0;D_c;D_O2;0;0;0;D_O2;0;0;0;D_O2;D_g;0;0;0;D_g;0;0;0;D_g];
36
37 %Geometric parameters
38 global xmax
39 global ymax
40 global zmax
41 global tmax
42 global allcentres
43 global Nclusters
44 global tstep
45
46 xmax = 1000 %um %1000
47 ymax = 1000 %um %1000
```

```

48 zmax = 100 %um %100
49 tmax = 51 %days %51
50 tstep = 3 %days %3
51
52 %must initialise random centres outside of initial function scope as it is
53 %called multiple times, and randomness within will confuse the solver
54 Nclusters = 3;
55 %allcentres = (0.25 + 0.5*rand(Nclusters ,3)).*[xmax,ymax,zmax]
56
57 %we use the same pregenerated random centres for consistency
58 allcentres = [553.7475, 578.2829, 39.4964; 597.1873, 640.3779, 65.8522; 415.7227, 253.0553, 43.7209]
59
60 %%%%%%%%%%%%%%%%%%%%%%%%%%%%%%%%%%%%%%
61 datetime('now')
62 tic %start timer
63
64 %create a pde object, and define the geometry of the problem
65 model = createpde(3);
66 [x,y,z] = meshgrid(0:xmax:xmax,0:ymax:ymax,0:zmax:zmax); %distances in um
67 t = 0:tstep:tmax; %time in days
68 x = x(:);
69 y = y(:);
70 z = z(:);
71 K = convhull(x,y,z);
72 nodes = [x';y';z'];
73 elements = K';
74 geometryFromMesh(model, nodes, elements);
75
76 % figure;
77 % pdegplot(model, 'FaceLabels','on','FaceAlpha',0.5); %plots the geometry for checking
78 % ax = gca;
79 % ax.XLim = [0,xmax];
80 % ax.YLim = [0,ymax];
81 % ax.ZLim = [0,zmax];
82 % xlabel('x / um');
83 % ylabel('y / um');
84 % zlabel('z / um');
85
86 %No flux of cells and nutrients through closed boundaries
87 applyBoundaryCondition(model,'neumann',...
88 % 'Face',1:6,...
89 % 'g',0,...
90 % 'q',0);
91
92 %oxygen and glucose through sides
93 applyBoundaryCondition(model,'dirichlet',...
94 % 'Face',[3,5],...
95 % 'h',[0,0,0;0,1,0;0,0,1],...
96 % 'r',[0,O2_0,g_0]);
97
98 %oxygen through top
99 applyBoundaryCondition(model,'dirichlet',...
100 % 'Face',6,...
101 % 'h',[0,0,0;0,1,0;0,0,0],...
102 % 'r',[0,O2_0,0]);
103
104 %specify the coefficients to make our system of equations
105 specifyCoefficients(model,'m',0,...
106 % 'd',[1;1;1],...
107 % 'c',c_coeffs,...
108 % 'a',0,...
109 % 'f',@source_func);
110
111 setInitialConditions(model,@init_func);
112 mesh = generateMesh(model,'Hmax',30);
113 result = solvepde(model,t);
114
115 toc %stop timer
116
117 tic %start timer

```

```

118
119 %prints out images of plots at given times
120 [X,Y,Z] = meshgrid(0:xmax/100:xmax,0:ymax/100:ymax,0:zmax/10:zmax);
121 U1 = interpolateSolution(result,X,Y,Z,1,1:length(t));
122 U1 = squeeze(U1);
123
124 for j=1:length(t)
125 t_fig = t(j);
126 fig_title = 'Cancer_Cell_Concentration_at_';
127 fig_title = fig_title + string(t_fig) + '_days';
128 U1_t = U1(:,j);
129 U1_t = reshape(U1_t, size(X));
130
131 h1 = figure('visible', 'off');
132 contourslice(X, ...
133 Y, ...
134 Z, ...
135 U1_t, ...
136 0:xmax/10:xmax, ...
137 0:ymax/10:ymax, ...
138 [0.25*zmax,0.5*zmax,0.75*zmax]);
139 ax1 = gca;
140 ax1.XLim = [0 ,xmax];
141 ax1.YLim = [0 ,ymax];
142 ax1.ZLim = [0 ,zmax];
143 xlabel('x/_um');
144 ylabel('y/_um');
145 zlabel('z/_um');
146 title(fig_title)
147 colormap jet;
148 c1 = colorbar;
149 c1.Label.String = 'u';
150 caxis([0 1]);
151
152 view(-45,45);
153 axis equal;
154 t_fig_str = strcat('u_t',num2str(t_fig));
155 print(h1,'-bestfit',t_fig_str,'-dpdf');
156 print(h1,t_fig_str,'-dpng');
157 close
158 end
159
160 toc %stop timer
161 tic %start timer
162
163 U2 = interpolateSolution(result,X,Y,Z,2,1:length(t));
164 U2 = squeeze(U2);
165
166 for j=1:length(t)
167 t_fig = t(j);
168 fig_title = 'Oxygen_Concentration_at_';
169 fig_title = fig_title + string(t_fig) + '_days';
170 U2_t = U2(:,j);
171 U2_t = reshape(U2_t, size(X));
172
173 h2 = figure('visible', 'off');
174 contourslice(X, ...
175 Y, ...
176 Z, ...
177 U2_t, ...
178 0:xmax/10:xmax, ...
179 0:ymax/10:ymax, ...
180 [0.25*zmax,0.5*zmax,0.75*zmax]);
181
182 ax2 = gca;
183 ax2.XLim = [0 ,xmax];
184 ax2.YLim = [0 ,ymax];
185 ax2.ZLim = [0 ,zmax];
186 xlabel('x/_um');
187 ylabel('y/_um');

```

```

188 zlabel('zu/um');
189 title(fig_title)
190 colormap jet;
191 c2 = colorbar;
192 c2.Label.String = 'O2u/umol';
193 caxis([0, 1.1*O2_0]);
194
195
196
197 view(-45,45);
198 axis equal;
199 t_fig_str = strcat('O2_t', num2str(t_fig));
200 print(h2, '-bestfit', t_fig_str, '-dpdf');
201 print(h2, t_fig_str, '-dpng');
202 close
203 end
204
205 toc %stop timer
206
207 tic %start timer
208
209 U3 = interpolateSolution(result, X, Y, Z, 2, 1:length(t));
210 U3 = squeeze(U3);
211
212 for j=1:length(t)
213 t_fig = t(j);
214 fig_title = 'Glucose_Concentration_at_';
215 fig_title = fig_title + string(t_fig) + '_days';
216 U3_t = U3(:,j);
217 U3_t = reshape(U3_t, size(X));
218
219 h3 = figure('visible', 'off');
220 contourslice(X, ...
221             Y, ...
222             Z, ...
223             U3_t, ...
224             0:xmax/10:xmax, ...
225             0:ymax/10:ymax, ...
226             [0.25*zmax, 0.5*zmax, 0.75*zmax]);
227
228 ax3 = gca;
229 ax3.XLim = [0, xmax];
230 ax3.YLim = [0, ymax];
231 ax3.ZLim = [0, zmax];
232 xlabel('xu/um');
233 ylabel('yu/um');
234 zlabel('zu/um');
235 title(fig_title)
236 colormap jet;
237 c3 = colorbar;
238 c3.Label.String = 'Glucoseu/mmol';
239 caxis([0, 1.1*g_0]);
240
241
242
243 view(-45,45);
244 axis equal;
245 t_fig_str = strcat('g_t', num2str(t_fig));
246 print(h3, '-bestfit', t_fig_str, '-dpdf');
247 print(h3, t_fig_str, '-dpng');
248 close
249 end
250
251 toc %stop timer
252
253 %%%%%%%%%%%%%%%%%%%%%%%%%%%%%%%%%%%%%%
254 %Source and initial condition functions defined here
255
256 function S = source_func(region, state)
257 %This defines the quadratic loss term for logistic proliferation with

```

```

258 %nutrition
259 global alpha
260 global K_o2
261 global v_o2
262 global K_g
263 global v_g
264 %
265
266 N=3;
267 nr = length(region.x);
268 S = zeros(N,nr);
269
270 %cf Michaelis Menten enzyme dynamics
271 O2_rate_prop = ((state.u(2,:)/(K_o2 + state.u(2,:)))) ;
272 glu_rate_prop = ((state.u(3,:)/(K_g + state.u(3,:)))) ;
273
274 S(1,:) = alpha*state.u(1,:)*(O2_rate_prop.*glu_rate_prop - state.u(1,:));
275 S(2,:) = -v_o2*O2_rate_prop.*state.u(1,:);
276 S(3,:) = -v_g*glu_rate_prop.*state.u(1,:);
277 end
278
279
280 function u_init = init_func(locations)
281 %This function defines the initial conditions of the problem
282 global O2_0
283 global g_0
284 global xmax
285 global ymax
286 global zmax
287 global allcentres
288 global Nclusters
289 %
290
291 c_0 = 0.01;
292 sigma = 10;
293 sigmaz = sigma*((zmax*zmax)/(xmax*ymax));
294
295 N=3;
296 M = length(locations.x);
297 u_init = zeros(N,M);
298 for i=1:Nclusters
299     %random start position of cell clusters
300     centre = allcentres(i,:);
301     %centre(3) = zmax/2;
302     u1_x = sqrt(2*pi)*sigma*normpdf(locations.x,centre(1),sigma);
303     u1_y = sqrt(2*pi)*sigma*normpdf(locations.y,centre(2),sigma);
304     u1_z = sqrt(2*pi)*sigmaz*normpdf(locations.z,centre(3),sigmaz);
305     u_init(1,:) = u_init(1,:) + c_0.*u1_x.*u1_y.*u1_z;
306 end
307
308 %uniform initial oxygen and glucose concentration
309 u_init(2,:) = O2_0;
310 u_init(3,:) = g_0;
311 end

```